Milestone #4 Report

Gaseous hydrogen permeation in X65 D pipeline steel and preliminary evaluation of the influence of oxygen on the inhibition of gaseous hydrogen embrittlement

02-April-2025

Project number: RP3.1-13

Milestone #4 report

Gaseous hydrogen permeation in X65 pipeline steel and preliminary evaluation on the influence of oxygen on the inhibition of gaseous hydrogen embrittlement

Authors:

Andrejs Atrens

Project team:

Maximilian Röthig, Joshua Hoschke, Md Fahdul Wahab Chowdhury, Clotario V. Tapia-Bastidas, Jeffrey Venezuela, Evan Gray, Tom Depover, Kim Verbeken, Milos B. Djukic, Andrej Atrens

Australian Government
Department of Industry, Science and Resources

Cooperative Research Centres Program

This work is funded by the Future Fuels CRC, supported through the Australian Government's Cooperative Research Centres Program. We gratefully acknowledge the cash and in-kind support from all our research, government and industry participants.

IMPORTANT DISCLAIMER

ACKNOWLEDGEMENT

The co-authors of the papers prepared for journal publication are thanked, as are the entities that provided support as indicated therein. This work is funded by the Future Fuels CRC, supported through the Australian Governments' Cooperative Research Centres Program. The cash and in-kind support from the industry participants is gratefully acknowledged.

PROJECT INFORMATION	
Project number	RP3.1-13
Project title	Feasibility of the use of gas phase inhibition of hydrogen embrittlement in gas transmission pipelines carrying hydrogen.
Research Program	3: Network Lifecycle Management
Milestone Report Number	4
Description	This work conducted permeation experiments through X65 D steel using hydrogen and hydrogen-oxygen mixtures at different pressures and contents of oxygen. The aim was to assess the effect of oxygen on the hydrogen permeation. A gas phase permeation apparatus was built and a model using the appropriate boundary conditions was derived. The findings include: - The derived balanced model of hydrogen permeation could reliably predict the measured permeation transients. The experimental parameters would allow the use of the ideal boundary conditions. - The measured hydrogen concentration was considerably lower than previously reported, and considerably lower than for Pd plated X65 D. This was likely due to the higher diffusivity. However, the measured steady state fluxes were only slightly lower than in previous works. - There was no effect of oxygen in the first set of experiments with a hydrogen pressure of 81 bar. - There was a slight effect of oxygen in the second set of experiments with a hydrogen pressure of 94 bar. The steady state flux was initially lower compared to pure hydrogen at the same pressure. However, the steady state flux slowly increased back to the level of pure hydrogen. The low hydrogen concentration evaluated in this work could have been to a lower steady state flux due to an oxide layer. However, the diffusion process was significantly faster. Furthermore, an already existing oxide layer might influence hydrogen permeation and, the detectability of the effect of oxygen on the hydrogen permeation. This report has been written as a paper for journal publication to ensure widest input and dissemination.
Research Provider	The University of Queensland (UQ)
Project Leader and Team	Andrej Atrens (UQ), Jeffrey Venezuela (UQ), Evan Gray (Griffith)
Industry Proponent and Advisor Team	**Tawake Rakai (AGIG)**, Guillaume Michal (APA), Mehdi Fardi (ROSEN), Jack Greenwood (DEM – SA Gov), Nick Kastelein (GPA Engineering), Tom Amrein (Jemena), Phil Colvin (Jemena), John Piper, Bradley Davis (UoW/ROSEN), Tim Aujard (AGIG), Michael Jarosz (SEA Gas), Eason Yi-Sheng Chen (Nanyang Technological University), Patrick Burr (UNSW), Sandra Kentish (University of Melbourne)
Related Commonwealth Schedule	RP3.1.1 Reports on the compatibility of current plastic and metallic network materials with future fuels delivered. RP3.1.2 New validated models to determine the long-term performance of materials for fuel transport delivered

Project start/completion date	1 Oct 2021 to 31 Dec 2026
IP Access	**Open** – The paper will be submitted for journal publication.
Approved by	Tawake Rakai, AGIG
Date of approval	April 2025

Table of Contents

Executive Summary

This preliminary work has been formulated as a paper for journal publication, as attached. This preliminary work conducted permeation experiments through X65 D steel using hydrogen and hydrogen-oxygen mixtures at different pressures and contents of oxygen. The aim was to assess the effect of oxygen on the hydrogen permeation and the effect of oxygen on the inhibition of gaseous hydrogen embrittlement. A gas phase permeation apparatus was built and a model using the appropriate boundary conditions was derived.

- The gas phase permeation cell using Pd plated X65 D has been used to measure the equilibrium hydrogen and hydrogen diffusivity. These values were consistent with literature values and were published in Hoschke et al, Corrosion Sci 243 (2025) 112580.
- The present work used X65 D surface activated in order to remove the surface oxide in order to study hydrogen permeation using an oxide free surface, and to study the effect of oxygen on the hydrogen entry and permeation through the X65 D.
- The measured hydrogen solubility was significantly lower than for the Pd coated X65 D, and the hydrogen diffusivity was considerably higher.
- The oxygen inhibition of hydrogen entry into the X65 D was quite small, much smaller than expected.

Implication for Industry

- Under the conditions of this study, there was little oxygen inhibition of hydrogen entry into X65 D.
- The implication is that there would be little oxygen inhibition of gaseous hydrogen embrittlement, under these conditions, which might imply a lack of reliability of oxygen inhibition.
- Future work is required to confirm or refute these preliminary findings.

Gaseous hydrogen permeation in X65 D pipeline steel and a preliminary evaluation of the influence of oxygen

Maximilian Röthig [a], Joshua Hoschke [a], Md Fahdul Wahab Chowdhury [a], Clotario V. Tapia-Bastidas [a,b], Jeffrey Venezuela [a], Evan Gray [c], Tom Depover [d], Kim Verbeken [d], Milos B. Djukic [e], Andrej Atrens [a,*]

[a] The University of Queensland, School of Mechanical and Mining Engineering, Centre for Advanced Materials Processing and Manufacturing (AMPAM), St. Lucia, Brisbane, Australia

[b] Faculty of Mechanical Engineering and Production Science, Escuela Superior Politécnica del Litoral (ESPOL), Guayaquil, Ecuador

[c] Queensland Micro- and Nanotechnology Centre, Griffith University, Nathan, Brisbane, Australia

[d] Ghent University, Department of Materials, Textiles and Chemical Engineering, Technologiepark 46, B-9052 Ghent

[e] University of Belgrade, Faculty of Mechanical Engineering, Kraljice Marije 16, Belgrade 11120, Serbia

[*] Corresponding author, andrejs.atrens@uq.edu.au, +61 7 3365 3748

Abstract

This paper reports on permeation experiments on X65 D steel using hydrogen and hydrogen-oxygen mixtures at different pressures and contents of oxygen. The aim was to assess the effect of oxygen on the hydrogen permeation. A gas-phase permeation apparatus was built and a model using the appropriate boundary conditions was derived. The findings include:

- The derived balanced model of hydrogen permeation could reliably predict the measured permeation transients. The experimental parameters would allow the use of the ideal boundary conditions.
- The measured hydrogen concentration was considerably lower than previously reported. This was likely due to the higher diffusivity. However, the measured steady state fluxes were only slightly lower than in previous works.
- There was no effect of oxygen in the first set of experiments with a hydrogen pressure of 81 bar.
- There was a slight effect of oxygen in the second set of experiments with a hydrogen pressure of 94 bar. The steady state flux was initially lower compared to pure hydrogen at the same pressure. However, the steady state flux slowly increased back to the level of pure hydrogen.

The low hydrogen concentration evaluated in this work could have been due to a lower steady state flux due to an oxide layer. However, the diffusion process was significantly faster. Furthermore, an already existing oxide layer might influence the detectability of the effect of oxygen on the hydrogen permeation. Future experiments should use a standardised method of specimen preparation that will effectively remove any residual oxide layer.

Keywords: Hydrogen embrittlement (HE), pipeline steel, hydrogen permeation, diffusion, oxygen inhibition, gas phase

1 INTRODUCTION

1.1 Background

Hydrogen typically decreases the mechanical properties of steel [1–5], a phenomenon known as hydrogen embrittlement (HE). HE is often studied using mechanical testing, which provides insight into the influence of the hydrogen dissolved in the steel. Hydrogen permeation testing allows understanding of the hydrogen uptake into the steel and hydrogen diffusion inside the steel. HE, if severe in the pipeline steel, could prevent hydrogen transport by a gas transmission pipeline.

The feasibility of repurposing existing natural gas pipelines for hydrogen transport and storage depends on the knowledge of the mechanical properties of the pipeline steel in contact with hydrogen, particularly the fracture toughness, strength and ductility. Hydrogen permeation experiments [6–8] or thermal desorption spectroscopy allow the evaluation of hydrogen charging conditions and hydrogen concentration inside the steel. In combination with mechanical testing [9–11] at those charging conditions, fitness-for-service assessments [12] can be made.

The service-life of converted infrastructure can be extended if the operational parameters are adjusted, such as pressure and throughput, or scheduled maintenance to minimise high pressure cycles. However, these modifications may impact the economic viability of the operation of the pipeline. Alternatively, newly installed pipeline segments could be coated with a hydrogen impermeable compound [13,14], but this would only effect a limited portion of the pipeline network and be susceptible to physical damage. Therefore, the addition of small amounts of an inhibitor gas to hydrogen has been proposed [15]. Research indicates [16] that the presence of gases such as oxygen [17] or carbon monoxide [18] may inhibit the adsorption of hydrogen onto the steel surface. Hydrogen uptake into the steel involves physical molecular adsorption on the surface, dissociation of the hydrogen molecule into hydrogen atoms and chemical adsorption of the hydrogen atoms, sub-surface absorption and bulk diffusion through the lattice and to trapping sites [19]. Gas-phase inhibition could mitigate hydrogen uptake by impedance of the hydrogen adsorption steps. Past work [20] has indicated that promising gaseous inhibitors have unsaturated bonds containing sulphur, carbon, or oxygen.

Staykov et al. [21] proposed a mechanism for inhibition of hydrogen uptake by oxygen in which dissociatively adsorbed oxygen increases the activation energy of hydrogen adsorption by decreasing the electron density at the steel surface.

The effectiveness of an hydrogen embrittlement inhibitor can be evaluated by the inhibition effectiveness, *E,* [16]

$$E = \frac{M_{\text{inhib}} - M_{\text{H}_2}}{M_{\text{inert}} - M_{\text{H}_2}} \cdot 100\ \% \qquad 1$$

where M_{inhib}, M_{H2}, and M_{inert} represent the measured mechanical property under the influence of the inhibitor gas, hydrogen, and in an inert atmosphere, respectively.

Hoffman and Rauls [22] were among the first to recognise the mitigating effect of oxygen. Their tensile tests on CK22 N steel, though not a pipeline steel, demonstrated a steady recovery in the reduction of area with increasing oxygen content in 100 atm hydrogen. As little as 10 ppm oxygen yielded an inhibition effectiveness of 38 %, which was increased to 83 % by 10,000 ppm oxygen.

Barthélémy and Pressouyre [23] conducted disk rupture tests using X70 pipeline steel. Oxygen contents of 120 ppm and 10,000 ppm increased the rupture pressure by 47 % and 74 %, compared to the rupture pressure using pure hydrogen.

Cialone and Holbrook [24] investigated the influence of carbon monoxide, sulphur dioxide, and oxygen on the fatigue crack growth rate of X42 in hydrogen, at a total pressure of 69 bar and at stress ratios of 0.1 and 0.8. Addition of 100 ppm oxygen completely inhibited the accelerated fatigue crack growth measured in pure hydrogen.

Kussmaul et al. [25] and Deimel et al. [26] investigated the tensile strength and fracture toughness of X70 pipeline steel in 90 bar hydrogen. The inhibition effectiveness for tensile tests was dependent on the strain rate. A high strain rate yielded higher effectiveness. A small oxygen content of 10 ppm had little-to-no effect (E = 0 –

22 %), whilst 150 ppm oxygen had a pronounced effect (E = 44 – 97 %) so that the tensile strength was the same as in air. However, the specimen in 150 ppm oxygen nevertheless had a small number of side cracks in the necking region, that were also present in pure hydrogen. The fracture toughness was measured as the J-integral at the 0.2 mm crack extension. There was no inhibition for 10 ppm oxygen. In contrast, 150 ppm oxygen led to almost complete inhibition (E = 98 %). The fracture surfaces for both the tensile and the fracture specimens were mixed mode, with quasi-cleavage fracture on the circumference of the specimen, indicating some effect of hydrogen, and ductile dimples on the inside.

Somerday et al. [27] measured the fatigue crack growth of X52 pipeline steel in 210 bar hydrogen. The addition of 10 ppm oxygen had no effect. However, 100 ppm and 1000 pm produced complete inhibition, though only up to a certain fatigue crack growth rate. They concluded that there was an inhibition effect when the rate of fatigue crack growth, either by increasing stress intensity factor or increasing test frequency, was restrained by the rate of oxygen adsorption onto the freshly created surfaces. When the fatigue crack growth rate was increased, the rate of passivation could not keep up, leading to an onset of accelerated fatigue crack growth despite the admixture of oxygen.

Ronevich et al. [28] measured fatigue crack growth and fracture toughness to assess the effectiveness of 100 ppm oxygen in 14 to 210 bar hydrogen on X100 pipeline steel. Depending on the test parameter (frequency, total pressure, stress ratio), oxygen had complete inhibition effectiveness up to a certain fatigue crack growth rate, similar to Somerday et al. [27]. Higher hydrogen pressures and higher frequencies led to an earlier onset while the influence of the stress ratio was not assessed. The fracture toughness tests revealed the dependency of the oxygen content. The oxygen concentration of 100 ppm was sufficient to produce an inhibition effectiveness of 100 % for a hydrogen pressure of 21 bar. However, the same oxygen content yielded only an inhibition effectiveness of 65 % at 210 bar hydrogen pressure.

Komoda [29] investigated the effect of oxygen admixtures on the fracture resistance of A333 pipeline steel in 6 bar hydrogen. The J-R curve in air aligned with the curve for 100 ppm oxygen, indicating complete inhibition effectiveness. Furthermore, the addition of 100 ppm oxygen caused the crack tip to retain the same shape as in air, and caused ductile fracture, comparable to the fracture in air.

These mechanical tests demonstrated the potential of as little as 100 ppm oxygen as an inhibitor of gaseous hydrogen embrittlement. The effectiveness strongly depended on test conditions such as strain rate, frequency or stress ratio, which may not directly translate to real service conditions. Moreover, inhibition effectiveness was related to oxygen content and partial pressure. While hydrogen embrittlement increased with increasing hydrogen partial pressure [30], it is likely that the required ratio of the oxygen content (and thus partial pressure) also scales accordingly to maintain its inhibitory effect.

The mechanism for oxygen inhibition is not clear. There appear to be various possibilities. Staykov et al. [21] found that oxygen molecules are captured by the steel surface deeper into the gas volume than hydrogen, attributed to the greater electronegativity and spatial orientation of the antibonding π* orbital. Nevertheless, the oxygen inhibition could be a kinetic effect or a thermodynamic effect. The work of Staykov et al. [21] suggests that the role of oxygen is to block the steel surface, so that some fraction of the steel surface, Θ, becomes impervious to hydrogen entry. In this case, it would be expected that the hydrogen solubility measured in a permeation experiment, C_{MB}, would be given by:

$$C_{\mathrm{MB}} = (1 - \Theta)\, C_{\mathrm{HSt}},$$

where C_{HST} is equilibrium hydrogen concentration in the steel in equilibrium with hydrogen gas of the pressure used in the measurement; and in a pipeline, the hydrogen solubility, C_{MP}, would be given by:

$$C_{\mathrm{MP}} = C_{\mathrm{HSt}}.$$

The alternative may be that the oxygen decreases the hydrogen fugacity at the steel surface to some fraction, $f_{O/H}$, of the hydrogen fugacity in the bulk hydrogen gas, by altering the hydrogen dissociation reaction at the steel surface, so decreasing the concentration of adsorbed hydrogen atoms at the steel surface, H_{ads}, so that the hydrogen concentration in the pipeline steel, C_{Mf}, would be given by:

$$C_{\mathrm{Mf}} = f_{\mathrm{O/H}}\, C_{\mathrm{HSt}}.$$

2 RESEARCH AIMS

This research aims to investigate the influence of small amounts of oxygen on the hydrogen permeation through X65 pipeline steel. A new gas-phase permeation apparatus was built to enable permeation experiments using pure hydrogen and hydrogen-based gas mixtures. The advantage of gas-phase permeation studies is that the permeability, and the diffusivity, of the steel membrane can be readily obtained from the measured data, enabling the evaluation of the solubility constant as well as the hydrogen concentration. In contrast, electrochemical hydrogen permeation experiments need careful calibration to establish the exact upstream conditions (i.e. hydrogen fugacity) and only yield the hydrogen diffusivity through the fitting of the transient hydrogen flux and the hydrogen concentration using the steady-state flux [31]. Furthermore, gaseous hydrogen charging allows investigation of gas mixtures.

Hydrogen entry into pipeline steels is impeded by the surface oxide that occurs on the steel surface after any exposure to air during specimen preparation [6]. This surface oxide is part of the oxygen inhibition effect. The impediment of oxide inhibition of hydrogen entry is overcome by immediate surface coating with palladium for experiments which measure the hydrogen solubility in the steel in equilibrium with hydrogen gas [6]. However, palladium plating cannot be used for experiments to study how oxygen influences gaseous hydrogen embrittlement. For that, an oxide-free steel surface is needed. An activation procedure was used by Venezuela et al. [32] that allowed hydrogen entry into the steel. The procedure was to make use of the fact that the oxide on the steel surface was reduced in the presence of hydrogen at a reasonable rate at 200 °C. That activation methodology was used in this research in order to attempt to produce a clean oxide-free steel surface for hydrogen permeation experiments and to study the effect of oxygen in the hydrogen gas.

This paper first describes the apparatus and the appropriate model that considers the initial and boundary conditions. Thereafter two series of experiments were carried out. The first series used the highest purity hydrogen readily available in Australia (99.999%). Baseline permeation experiments with pure hydrogen were conducted first. Thereafter, the permeation experiments were conducted using hydrogen containing 100, 300 and 1000 ppm oxygen. The second series used extremely pure (99.99999 %) hydrogen from a mischmetal-Ni_5 metal-hydride source.

3 METHODOLOGY

3.1 Gas-phase permeation apparatus

In the gas-phase permeation method, a specimen (membrane) is charged with gaseous hydrogen on the feed side (upstream). The hydrogen permeates through the membrane by diffusion and is detected on the permeate side (downstream). This study monitored the hydrogen permeation by the pressure increase in a fixed known measuring volume, rather than using electrochemical methods or mass spectroscopy. The pressure was measured using a heated capacitance manometer (Kurt J. Lesker, HCG045-KT-6-1) with a full-scale of 1 Torr. A schematic of the apparatus controlling the gas composition and pressure to the gas phase permeation cell is shown in Figure 1. The gas-phase hydrogen permeation cell is presented in Figure 2 and Figure 3.

The apparatus allowed pure hydrogen to be introduced into the permeation cell directly from either a gas cylinder or a metal-hydride compressor [https://doi.org/10.1088/2515-7655/ab9314] capable of generating > 200 bar. Alternatively, a gas mixture can be prepared beforehand and expanded into the permeation cell. The system featured multiple gas inlets connected to a manifold and two sample cylinders. Each volume was calibrated and fitted with pressure transmitters and thermocouples to determine the gas quantity at each step. After each expansion step, adequate time was allowed for the gas to reach thermal equilibrium at room temperature.

To prepare a gas mixture, hydrogen was first charged into the sample cylinders. Then, the manifold was evacuated using a roughing vacuum pump. Oxygen gas was introduced into its designated inlet volume at an appropriate pressure to achieve the desired oxygen concentration in the hydrogen gas. Oxygen was expanded into the manifold and mixed by opening the valves to the hydrogen-filled sample cylinders. The pressure and temperature of the hydrogen and oxygen in their respective volumes were measured just before mixing. The mixing ratio, Q, was calculated using

$$Q = \frac{n_{O_2}}{n_{H_2} + n_{O_2}}. \qquad 2$$

where n_{O2} and n_{H2} represent the amount of gas (mol), O_2 and H_2, respectively, calculated using the real gas law. The hydrogen–oxygen mixtures are described later. Care was taken to ensure the mixture was outside the flammability limits. The upper flammability limit of hydrogen in pure oxygen is 95 vol% [33] and all tested mixing ratios *Q* were well below this 5 % limit.

The permeation cell was constructed from type A-286 (UNS S66286) iron-nickel-chromium super alloy and was hydrostatically pressure tested to 250 bar. The cell was sealed using a two-stage O-ring design. Two small O-rings sealed the upstream and downstream volume against the disc specimen and the two flanges. A larger O-ring created a seal between the two flanges. The O-rings were made of Viton, a high-temperature-resistant compound. For membranes with low permeability, outgassing of the O-rings and gas permeation through them could significantly affect the measurements over time. Therefore, it was essential to heat the O-rings under vacuum for a prolonged period to allow outgassing. To mitigate the effect of hydrogen permeation through the O-rings, a guard vacuum was created between the two O-ring stages. This effectively removed any residual gas trapped between the stages during assembly and any hydrogen that might permeate during an experiment. Despite these precautions, there was a small background flux. Hence, a correction term was incorporated into the model as described later.

The permeation cell was connected to the apparatus using fittings that were brazed to the cell, allowing high-temperature heating. The cell was also fitted with two valves on either side, enabling assembly inside a glove box to minimise exposure of the specimen surfaces to air.

After assembly, the background pressure was measured without pumping the downstream volume. A helium leak test was performed afterwards. As Viton is permeable to helium while the steel specimen is not, a leak would have caused a pressure increase higher than the previously measured background-pressure. In both cases, there was only a minor gas load in the order of 10^{-8} mbar L s^{-1}. This could be attributed to the unpumped volume during measuring. The measured gas load was a linear pressure increase without the characteristic S-shaped curve that would suggest helium permeation through the outgassed O-rings. This confirmed the leak-free integrity of the cell and the effectiveness of the vacuum sealed O-rings.

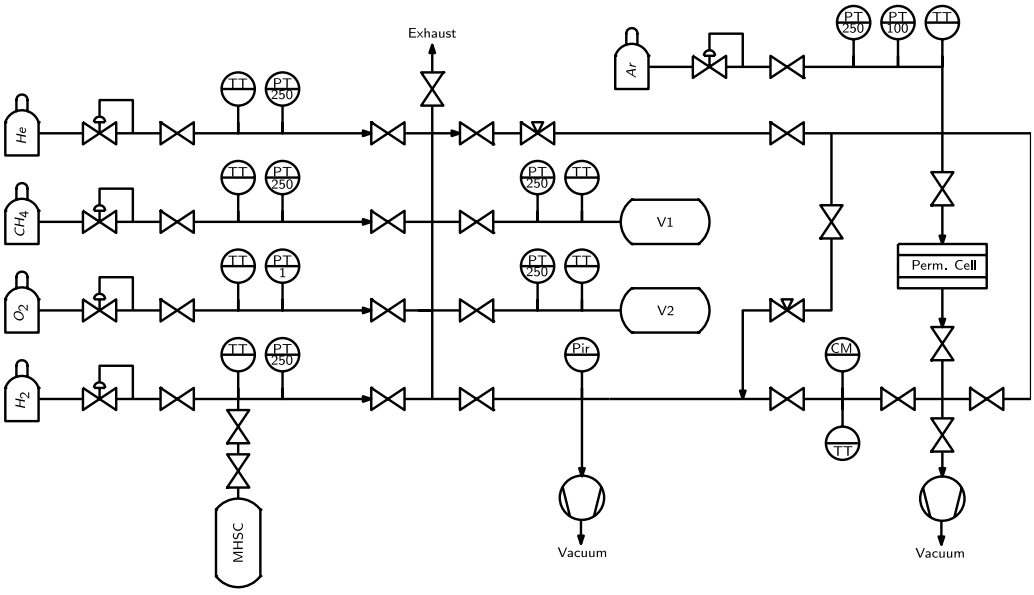

Figure 1 Piping and instrumentation diagram of the gas-phase permeation apparatus. PT denotes a pressure transmitter, TT a temperature transmitter, V1 and V2 are the sample cylinders used to prepare gas mixtures, MHSC is the metal hydride sample cylinder, Pir is the Pirani gauge, and CM is the capacitance manometer (1 Torr full scale).

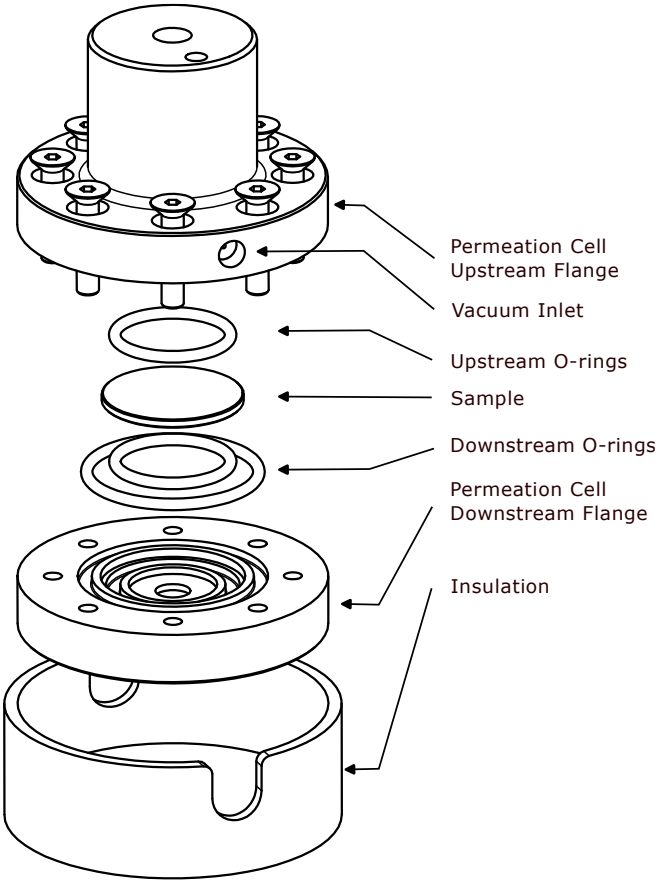

Figure 2 Exploded assembly view of the cell used for the permeation experiments. The band heater is not shown.

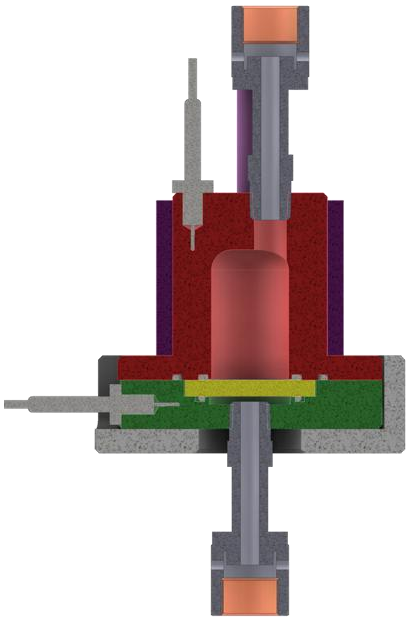

Figure 3 Schematic of the gas-phase hydrogen permeation cell. The specimen is indicated in yellow, 2 mm thickness, diam 32 mm.

3.2 Model Description

The mass transport across a membrane is governed by the diffusion equation, commonly known as Fick's second law [34], that relates the change in concentration, *c*, over time to the second spatial derivative of the concentration. The proportionality constant *D* is the diffusivity of the material and may be interpreted as a measure of the speed of diffusion.

$$\frac{\partial \mathrm{c}}{\partial t} = D\frac{\partial^2 \mathrm{c}}{\partial x^2} \tag{3}$$

A well-established approach to determine the hydrogen diffusivity is to analyse the hydrogen flux [35–37]. The diffusivity can be estimated using the time-lag method [38,39], the breakthrough time [7], or by fitting the entire permeation curve [6] to a solution of Eq. 3. Typically, these methods assume the following ideal initial and boundary conditions

$$\begin{aligned} c(x,0) &= 0 && 0 \le x \le L \\ c(0,t) &= c_1 = \text{const.} && t \ge 0 \\ c(L,t) &= c_2 = 0 && t \ge 0 \end{aligned} \tag{4}$$

where *L* is the membrane thickness. The indices 1 and 2 denote the feed and permeate side, respectively. Under these conditions, the hydrogen flux during a rise and decay transient can be described [40] as

$$\frac{J(t) - J_0}{J_\infty - J_0} = 1 + 2\sum_{n=1}^{\infty}(-1)^n \exp\left(-\frac{Dn^2\pi^2 t}{L^2}\right) \tag{5}$$

and

$$\frac{J(t) - J_\infty}{J_0 - J_\infty} = -2\sum_{n=1}^{\infty}(-1)^n \exp\left(-\frac{Dn^2\pi^2 t}{L^2}\right) \tag{6}$$

where J_∞ and J_0 are the steady state and the initial hydrogen fluxes, respectively. If a decay experiment follows a rise transient immediately, then J_0 equals J_∞.

This work used a fixed downstream volume, so that the measured downstream hydrogen pressure increased over time. As a result, the boundary conditions deviated from the ideal case. To address this, a model was developed to reflect the real initial and boundary conditions of this experimental setup, as illustrated in Figure 4. Unlike most other experimental setups that measure the hydrogen flux directly [35], this apparatus measured the downstream hydrogen pressure over time. The flux can be deduced as the time-derivative of the measured pressure. However, differentiation is a noise amplifier. Thus, the goal was to derive an equation that could be directly fitted to the measured pressure. The initial and boundary conditions of this model are:

$$\begin{aligned} \mathrm{c}(x,0) &= f(x) && 0 \le x \le L \\ \mathrm{c}(0,t) &= c_1 = \text{const.} && t \ge 0 \\ \mathrm{c}(L,t) &= c_2 = f(t) && t \ge 0. \end{aligned} \tag{7}$$

Given that the feed pressure was at least four orders of magnitude higher than the permeate pressure, the upstream concentration c_1 was assumed to be constant. As hydrogen permeates into the downstream volume, c_2 increases over time, theoretically never reaching a true steady state. Additionally, a variable initial concentration profile was introduced to model subsequent transients based on the previously attained concentration profile. Using Carslaw's solution [41] to Eq. 3, the concentration profile as a function of position *x*, and time *t* is:

$$\mathrm{c}(x,t) = c_1 + (c_2 - c_1)\frac{x}{L} \tag{8}$$

$$+\frac{2}{L}\sum_{n=1}^{\infty}\sin\frac{n\pi x}{L}\exp\left(-\frac{Dn^2\pi^2 t}{L^2}\right)\cdot\int_0^x f(x')\sin\frac{n\pi x'}{L}\,dx'.$$

The initial concentration profile is modelled as

$$\mathrm{c}(x,0)=c_{1,0}\left(1-\frac{x}{L}\right)+c_{2,0}\left(\frac{x}{L}\right) \qquad 9$$

where $c_{1,0}$ and $c_{2,0}$ represent the initial upstream and downstream concentrations at t_0. Setting both initial concentrations to zero gives the solution for a hydrogen-free specimen. It should be noted that this profile assumes a steady state condition, when the concentration profile has become linear. Therefore, consecutive experiments, such as a rise transient followed by a decay transient, should be long enough that steady state is attained. Furthermore, in the case where c_2 is a function over time, equilibrium between c_1 and c_2 should be reached. By solving Eq. 8 with Eq. 9, the concentration profile becomes:

$$\begin{aligned}c(x,t)&=c_1+(c_2-c_1)\frac{x}{L} \qquad 10\\&+\frac{2}{\pi}\sum_{\mathrm{n}=1}^{\infty}\frac{\mathrm{c}_2\cos\mathrm{n}\,\pi-\mathrm{c}_1}{\mathrm{n}}\sin\frac{n\pi x}{L}\cdot\exp\left(-\frac{\mathrm{Dn}^2\pi^2 t}{L^2}\right)\\&+\frac{2}{\pi}\sum_{n=1}^{\infty}\frac{c_{1,0}-c_{2,0}\cos n\,\pi}{n}\sin\frac{n\pi x}{L}\cdot\exp\left(-\frac{\mathrm{Dn}^2\pi^2 t}{L^2}\right).\end{aligned}$$

According to Fick's first law [34], the hydrogen flux is given by:

$$J=D\frac{\mathrm{d}c}{\mathrm{d}x}. \qquad 11$$

Differentiating Eq. 10 with respect to x and evaluating at $x = L$ yields the hydrogen flux at the permeate side:

$$\begin{aligned}J_{\mathrm{L}}(\mathrm{t})&=D\frac{\mathrm{c}_1-\mathrm{c}_2}{L} \qquad 12\\&-\frac{2D}{L}\sum_{n=1}^{\infty}(\mathrm{c}_2-\mathrm{c}_1\cos n\,\pi)\cdot\exp\left(-\frac{Dn^2\pi^2 t}{L^2}\right)\\&-\frac{2D}{L}\sum_{n=1}^{\infty}\left(c_{1,0}\cos n\,\pi-c_{2,0}\right)\cdot\exp\left(-\frac{Dn^2\pi^2 t}{L^2}\right).\end{aligned}$$

Applying Sieverts' law [42]

$$c_{\mathrm{H}}=\mathrm{S}\cdot\sqrt{p} \qquad 13$$

leads to the modified flux for gaseous permeation

$$J_{\mathrm{L}}(t)=\mathrm{DS}\frac{\sqrt{p_1}-\sqrt{p_2}}{L} \qquad 14$$

$$-\frac{2\mathrm{DS}}{L}\sum_{n=1}^{\infty}\left(\sqrt{p_2}-\sqrt{p_1}\cos n\,\pi\right)\cdot\exp\left(-\frac{Dn^2\pi^2t}{\mathrm{L}^2}\right)$$
$$-\frac{2\mathrm{DS}}{L}\sum_{n=1}^{\infty}\left(\sqrt{p_{1,0}}\cos n\,\pi-\sqrt{p_{2,0}}\right)\cdot\exp\left(-\frac{Dn^2\pi^2t}{L^2}\right).$$

Here, the product of the diffusivity D and the solubility constant S is the permeability Φ [31]. Eq. 14 can be interpreted as a superposition of three flux components: the steady state flux, the transient flux due to the boundary conditions, and the decaying transient flux due to the initial conditions (previous boundary conditions).

The hydrogen flux can be converted to the change in pressure considering the mass balance across the membrane

$$J_{\mathrm{L}}=\frac{2}{A}\cdot\frac{\mathrm{d}n_2}{\mathrm{d}t}=\frac{2}{A}\cdot\frac{V_2}{RTZ}\cdot\frac{\mathrm{d}p_2}{\mathrm{d}t} \qquad 15$$

where $\mathrm{d}n_2/\mathrm{d}t$ is the change in the amount of hydrogen over time, A is the exposed area of the membrane, $\mathrm{d}p_2/\mathrm{d}t$ is the change of pressure over time, V_2 is the downstream volume, R is the universal gas constant, T is the temperature measured in V_2, and Z is the compressibility factor of the accumulating hydrogen gas. The factor of two accounts for the conversion from atomic to molecular hydrogen flux [43]. Finally, integration of Eq. 15 gives the pressure as a function of time:

$$p_2(t)=\frac{A}{2}\cdot\frac{RTZ}{V_2}\cdot\int_0^{\mathrm{t}}J_{\mathrm{L}}\,\mathrm{d}t'+t\cdot\left(\frac{\mathrm{d}p_2}{\mathrm{d}t}\right)_0+p_{2,0}. \qquad 16$$

The constant of integration is added as $p_{2,0}$ which is the base-pressure at the start of the experiment. The initial flux $(\mathrm{d}p_2/\mathrm{d}t)_0$ may account for a linear background flux that may arise due to leakages of the unpumped volume during the experiment or residual outgassing of the membrane.

To determine diffusivity, permeability, and the solubility constant, Eq. 16 is fitted to the measured pressure data by integration of the hydrogen flux described in Eq.14. The model includes a feedback loop to account for the influence of previous downstream pressures. Unlike traditional methods that depend on flux normalisation or fitting a linear segment of the pressure curve to determine the time-lag, this approach avoids the ambiguity of selecting flux values and the difficulty of identifying a suitable linear region. Hereinafter, Eq. 16 is denoted as the balanced model.

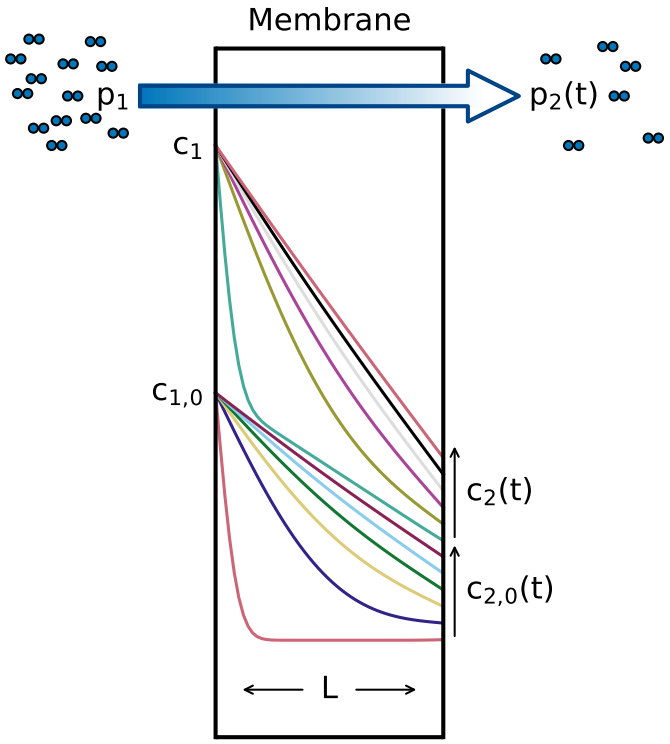

Figure 4 Schematic of the permeation model. The coloured lines depict the concentration profile inside the membrane over time, where each line represents a distinct time. The initial concentration $c_{1,0}$ causes the downstream concentration $c_{2,0}$ to rise over time. In a subsequent experiment, the upstream concentration is increased to c_1. The downstream concentration c_2 adjusts accordingly. Due to the accumulation of hydrogen on the feed side of the membrane, the downstream pressure and thus the hydrogen concentration increase steadily.

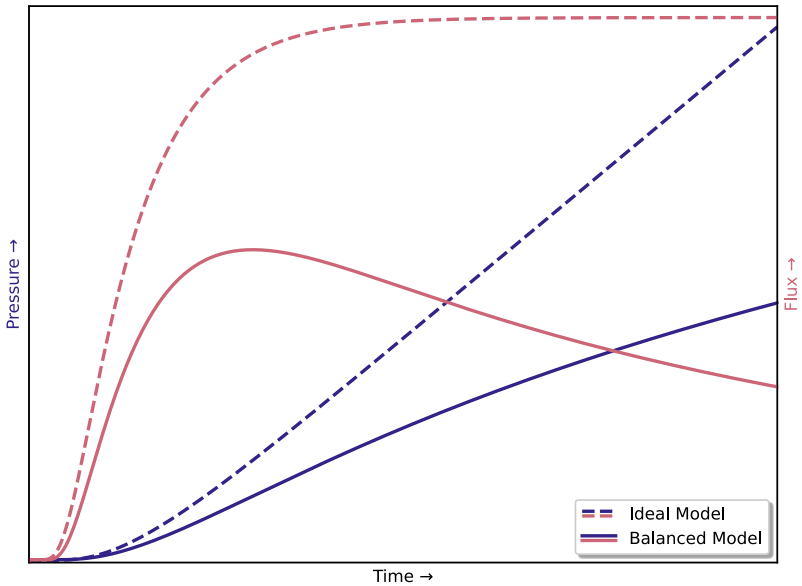

Figure 5 Schematic comparison of the resulting pressure (blue) and flux (red) between the ideal and the balanced model. In the ideal model, the permeate concentration stays constant. Thus, the pressure increases at a steady rate as depicted with the dashed line. This, however, would violate the real boundary conditions where the static volume leads to an increasing pressure and a change in permeate concentration. The balanced model (solid lines) reflects this situation, showing an inflection point in the pressure and flux. At infinite time, the pressure would equalise and reach the upstream pressure. At that time, the flux would decrease to zero.

3.3 Experimental

The investigated material was a vintage X65 steel (1980), designated as X65 D, extracted from the Dampier Bunbury natural gas transmission pipeline (DBNGP). In prior research, the material was characterised [9,11] and the tensile properties [11] and fracture toughness [10] under hydrogen exposure were studied. The chemical composition is presented in Table 1. The microstructure was composed of banded ferrite and pearlite. The banding was stacked in the radial direction and elongated in the transverse and longitudinal direction, corresponding to the rolling direction.

Table 1 Composition of the X65 D vintage steel in weight percent. The balance is Fe.

C	Si	Mn	P	S	Al	Cr	Mo	Ni	Co	Cu	Nb	Ti	V
0.12	0.26	1.51	0.02	0.006	0.033	0.02	0.01	0.01	0.003	0.01	0.04	0.001	0.005

The permeation experiments used a disc with a diameter of 32 mm and a thickness of 2 mm, extracted from a pipeline section. The specimen thickness was in the radial direction of the pipe. The specimen was ground to 600 on both sides. The specimen was moved into a glovebox and the surface preparation was continued under an argon atmosphere. The specimen was ground to 1200 grit and the permeation cell was assembled inside the glovebox. Two valves on either side of the cell ensured that the specimen was not exposed to air when the cell was taken out of the glovebox and fitted into the apparatus.

During this specimen preparation, the oxygen content in the argon was less than 0.1 ppm. This equates to 10^{-4} mbar oxygen. However, as argon is not attracted to the steel surface, there was likely a thin oxygen film. Thus, a subsequent surface activation was performed. The assembled permeation cell was evacuated from the argon atmosphere. The cell was heated to 150 °C for 24 h under constantly pumped vacuum to outgas the O-rings. Following, the cell was heated to 200 °C for 24 h with an upstream hydrogen pressure of 50 bar and a downstream hydrogen pressure of 38 bar. This was to reduce any oxides that might have formed during preparation. While the specimen was still being heated, the gas was evacuated for 2 h ensuring all absorbed hydrogen was released. Then, the cell was cooled to room temperature under vacuum.

Table 2 Operating conditions.

Parameter	**Symbol**	**Unit**	**Value**
sample thickness	*L*	m	0.0020
exposed membrane area	*A*	m^2	0.000441
downstream volume	*V*	m^3	0.0000207
temperature	*T*	°C	23 ± 1
hydrogen purity	-	-	99.999 % (compressed gas cylinder) > 99.999 % (metal hydride source)

All experiments were performed at 23 ± 1 °C. The permeation experiments were conducted either using ultra-high purity hydrogen (99.999 %) from a compressed gas cylinder (CGC) with a specified oxygen concentration of less than 2 ppm, or with hydrogen from a metal hydride source (MHSC). Desorbed hydrogen from a metal hydride source is estimated to have much higher purity than ultra-high purity hydrogen from a compressed gas cylinder (CITE). However, the actual purity was not measured. The operating conditions are summarised in Table 3.

Three pressure levels were tested using pure hydrogen from the compressed gas cylinder. At each pressure level, three transients were conducted to minimise the influence of potential trapping effects [44]. Between each pressure level the specimen was heated to 150 °C for 4 h under vacuum to replicate the initial starting conditions. However, between each rise transient at the respective pressure, the specimen was only allowed to desorb for

100 min at room temperature. The intention was to keep the strong traps filled and to remove only lattice hydrogen and potentially hydrogen from lower energy (weak) traps.

Two sets of hydrogen-oxygen permeation experiments were conducted. The first set of experiments was at a total pressure of 81. The specimen was not heated prior to this test. There was a single rise transient at 81 bar using pure hydrogen (CGC), followed by an extended decay transient. This served as the baseline result. Subsequently, the hydrogen-oxygen tests used increasingly higher oxygen concentrations. There was no heating between the oxygen experiments.

The second set of experiments was conducted at a total pressure of 94 bar using hydrogen sourced from the metal hydride reservoir. Prior to the tests, the described specimen preparation was repeated in the glovebox. The specimen was then heated to 150 °C under vacuum for 12 h to allow sufficient time for outgassing of the O-rings. One rise and one extended decay transient was measured using pure hydrogen (MHSC). In the following experiments, only rise transients were measured. After each subsequent experiment, the specimen was heated to 50 °C to allow fast hydrogen desorption. After the experiments containing 100 ppm and 5000 ppm oxygen, respectively, there was one experiment where the feed side of the specimen was exposed to air for 1 hour. The air was evacuated before the specimen was charged with pure hydrogen. In the subsequent experiment, the feed side of the specimen was exposed to 3.4 bar pure oxygen for roughly 4 minutes. This was equivalent to the exposure of 1 bar of air for 1 h from the previous experiment. Then, pure hydrogen was charged to the specimen without removing the pure oxygen, resulting in an oxygen content of 12000 ppm. The final experiment used pure hydrogen only. This was to confirm the removal of oxygen from the previous experiments.

Table 3 Test matrix for hydrogen, and hydrogen-oxygen permeation experiments.

Type (source)		Total pressure (bar)	Oxygen content (ppm)	Transients	Heating
H_2		121	0	3 rise, 3 full decay	200 °C prior
		65	0	3 rise, 3 full decay	150 °C prior
		25	0	3 rise, 3 full decay	150 °C prior
H_2-O_2	(CGC)	81	0	1 rise, 1 decay	No heating
			100	1 rise, 1 decay	No heating
			300	1 rise, 1 decay	No heating
			1000	1 rise, 1 decay	No heating
	(MHSC)	94	0	1 rise, 1 decay	150 °C prior
			100	1 rise	No heating
			5000	1 rise	50 °C prior
			air exposure	1 rise	50 °C prior
			12000	1 rise	50 °C prior
			0	1 rise	50 °C prior

4 RESULTS

4.1 Pure Hydrogen

Figure 6 shows a typical example of the measured pressure and the fitted models for a rise and a decay transient. The error of the fit to the recorded rise transient was less than 1 %, evaluated as the normalised root mean square error. The error of fit of the flux, Figure 7, was generally higher, attributed to the noisiness of the flux (light blue area), derived by differentiation of the recorded pressure.

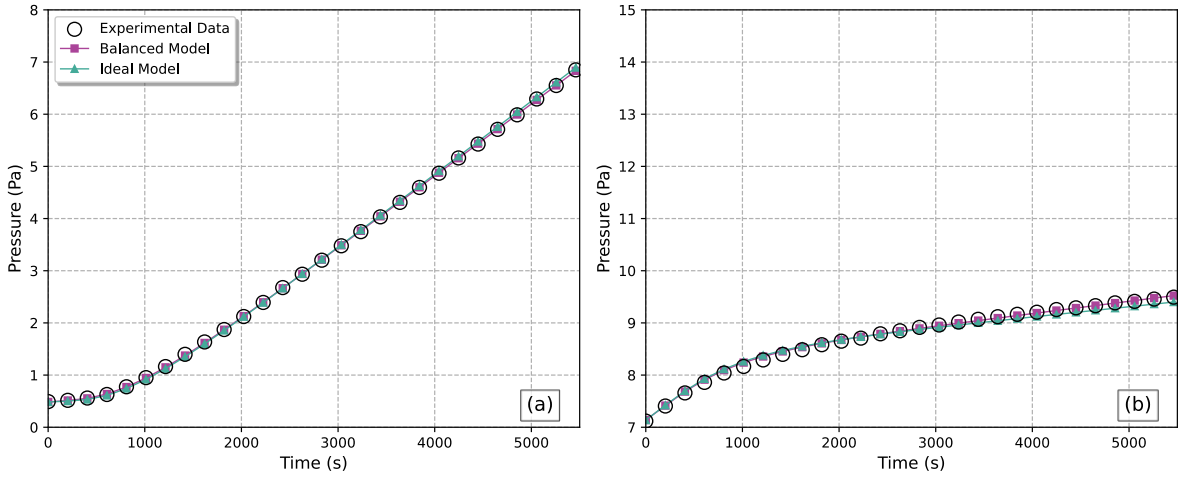

Figure 6 Experimental pressure and fit curves for the balanced and ideal models. The presented data is from the second rise and decay transients with an upstream hydrogen pressure of 65 bar.

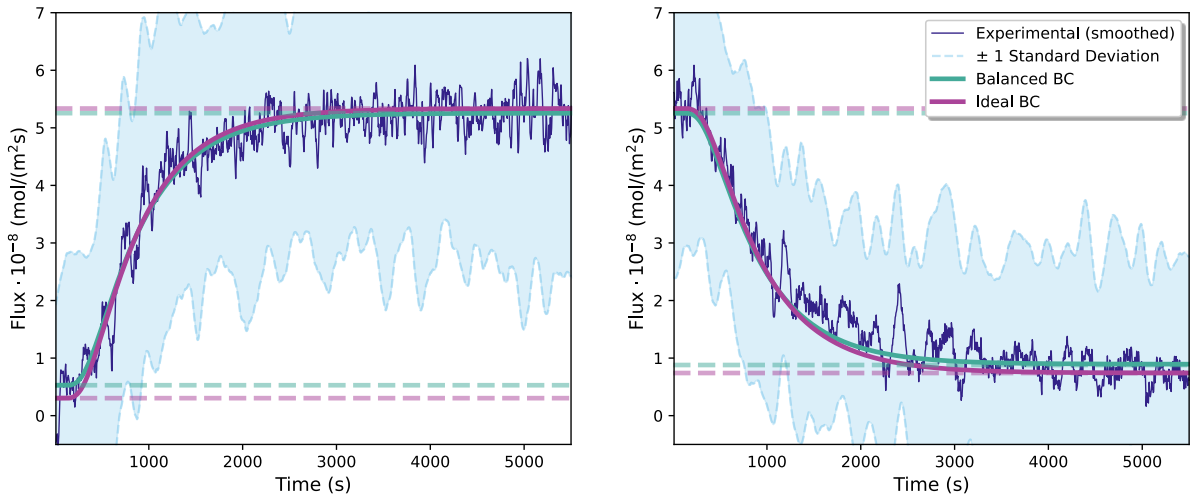

Figure 7 Experimental flux and fit curves for the balanced and ideal models. The presented data is from the second rise and decay transients with an upstream hydrogen pressure of 65 bar. The light blue underlay is one standard deviation of the mean of the experimental flux. The dark blue line is the moving average of the experimental flux with a window size of 25.

All rise transients using pure hydrogen are presented in Figure 8. The fitted diffusion parameters are summarised in Table 4 for the balanced model and in Table 6 for the ideal model. The recorded pressure is shown in Figure 8(a), while the pressure that is adjusted for the fitted background flux is depicted in Figure 8(b). In both figures, the measured pressure increased as the upstream hydrogen pressure increased. In Fig. 7(a), the absolute pressure increase was lower for the first transient at each pressure level, compared to the second or third transient. This indicates that permeation was affected by hydrogen trapping. As there was no heating between each transient, most traps were filled when the second and third transient commenced, resulting in a slightly faster rise of the recorded pressure. This effect was most pronounced at 121 bar.

The resulting flux, obtained by differentiation of the modelled pressure, is presented in Figure 8(c) and (d). The unadjusted flux (Fig. 8(c)) was expected to approach a common steady state flux according to Eq. 11. While this occurred for 25 bar and 65 bar, the 121 bar transients were different and the steady state flux increased with the experiment number. This was also measured by Koren et al. [7], who measured a similar increase using X65, where the flux of the third transient for upstream pressures of 10 bar and 100 bar were higher than the previous transient.

The normalised flux in Fig. 8(d) shows slower diffusion for the first transient compared to the second and third transient. This agrees with the observation of Figure 8(a). At an upstream pressure of 25 bar, all transients were slower than those for 65 bar and 121 bar. While the first transient was still lagging, even the second and third transients experienced a slower diffusion than the first transients of the high-pressure levels. Similarly, Koren et al. [7] found that their normalised flux transients were also slower the lower the upstream pressure.

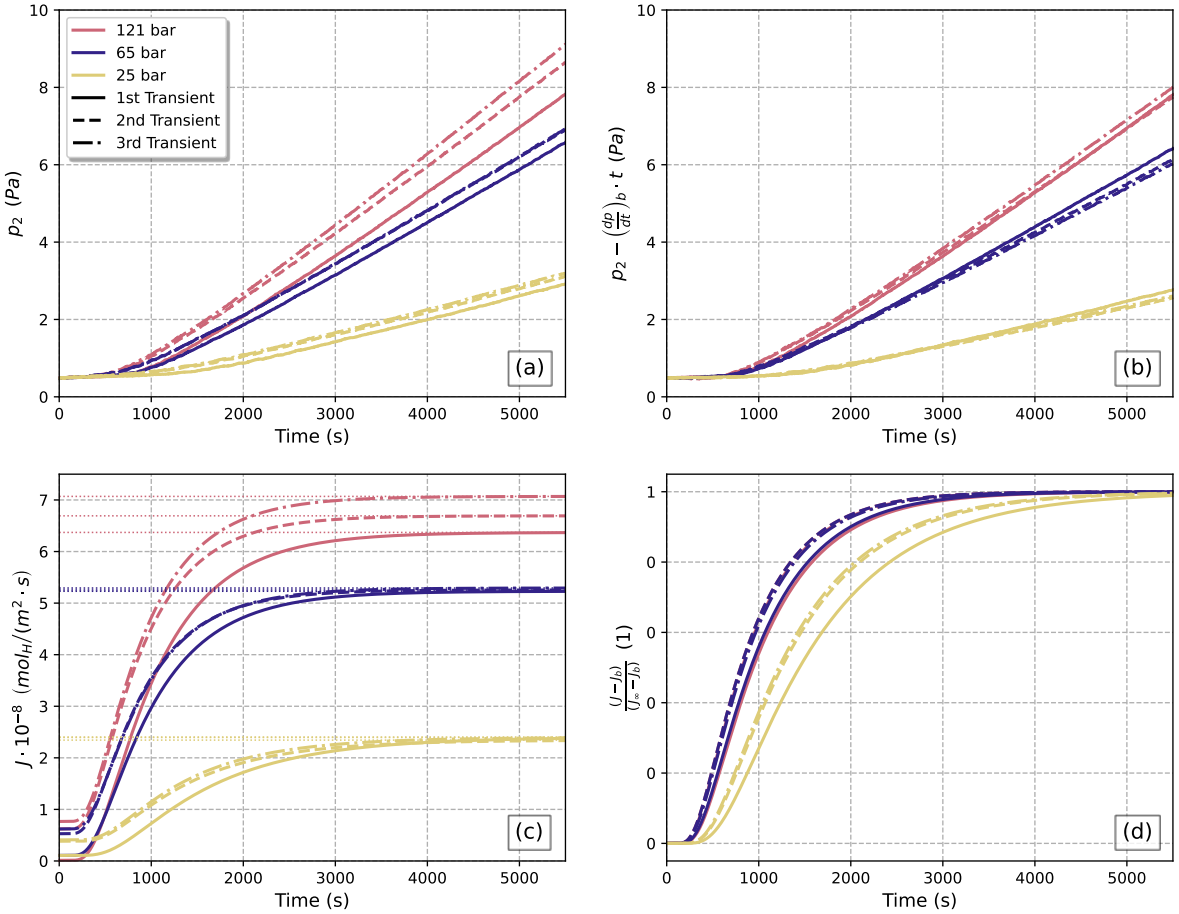

Figure 8 Measured pressure (a, b) and fitted flux (c, d) of all pressure levels tested with pure hydrogen and the respective transients. (a) Recorded pressure. (b) Recorded pressure adjusted for the fitted background flux. (c) Recorded flux and the steady state flux (dotted lines). (d) Normalised flux.

Table 4 Summary of the diffusion parameters evaluated from the rise transients using the balanced model. The normalised root mean square error (NRMSE) is based on both the recorded pressure, p, and flux, J.

Pressure (bar)	Trans.	D_{app} (10^{-10} m^2/s)	S (10^{-5} $mol/m^3/Pa^{0.5}$)	Φ (10^{-14} $mol/m/s/Pa^{0.5}$)	J_∞ (10^{-8} $mol/m^2/s$)	J_b (10^{-9} $mol/m^2/s$)	NRMSE (%) p	NRMSE (%) J
121	1	5.90	6.20	3.66	6.37	0.12	0.23	11.0
	2	6.93	5.06	3.50	6.69	6.22	0.24	13.1
	3	6.78	5.35	3.62	7.07	7.66	0.23	10.8
65	1	6.08	6.61	4.02	5.23	1.08	0.20	10.6
	2	6.92	5.33	3.69	5.26	5.29	0.16	12.1
	3	6.71	5.46	3.66	5.29	6.20	0.18	14.4
25	1	3.85	7.55	2.91	2.40	1.07	0.45	13.2
	2	4.45	5.60	2.49	2.34	3.83	0.28	9.4
	3	4.56	5.55	2.53	2.40	4.09	0.24	13.0

Figure 9 presents the steady-state flux as a function of the square-root of hydrogen fugacity. Fugacity is the thermodynamic activity of the gas [43] and is measured in units of pressure. For hydrogen gas pressures less than 200 bar, the difference between hydrogen pressure and hydrogen fugacity is small, but can be evaluated easily. Combining Eq. 11 and Eq. 13 gives the flux as a function of permeability

$$J(\mathrm{t}) = \frac{\Phi}{L}\left(\sqrt{f_1} - \sqrt{f_2(\mathrm{t})}\right) \qquad 17$$

with

$$\Phi = DS \qquad 18$$

where f_1 and f_2 are the fugacities evaluated from the upstream and downstream pressures. Eq. 17 indicates that the slope of a linear regression line through the adjusted flux as a function of the square root of fugacity equals the permeability divided by the sample thickness. Though permeability can be evaluated using a single transient, using the linear regression line gives an average value across all pressure levels. The evaluated permeability constants listed in Table 4 are presented in Figure 10.

The hydrogen concentration in equilibrium with the upstream pressure can be evaluated using Fick's first law (Eq. 11) or Sieverts' law (Eq. 13). Figure 11 shows the hydrogen concentration, calculated using both methods using the respective values obtained by fitting the individual transients. The linear regression lines for each number of transients have a positive intercept with the ordinate, following the modified Sieverts' law [32]

$$c_{\mathrm{H}} = S \cdot \sqrt{p} + c_{\mathrm{T}} \qquad 19$$

where c_T is the concentration of trapped hydrogen. However, the intercepts decreased with increasing number of transients, signifying the trapping effect. Therefore, the lattice solubility constant was approximated as the mean of the third transient. Then, the hydrogen lattice concentration is given by Eq. 13 using the mean solubility constant. The average permeability, solubility constant, and, by extension, diffusivity, are given in Table 5. The reported diffusivities in this work are well below the diffusivity of pure iron (3.2×10^{-9} m/s^2 [45] to 7.3×10^{-9} m/s^2 [46]). It should be noted that for the second and third transients, the initial flux contributes to the steady state flux. As the balanced model uses the adjusted flux to derive the permeability and solubility constant, the concentration based on Sieverts' law might be underestimated. The lower values of diffusion coefficient measured in this work are attributed to the substantial amount of hydrogen traps. This is consistent with the positive intercept for the plots of hydrogen equilibrium concentration plotted against the square root of hydrogen fugacity.

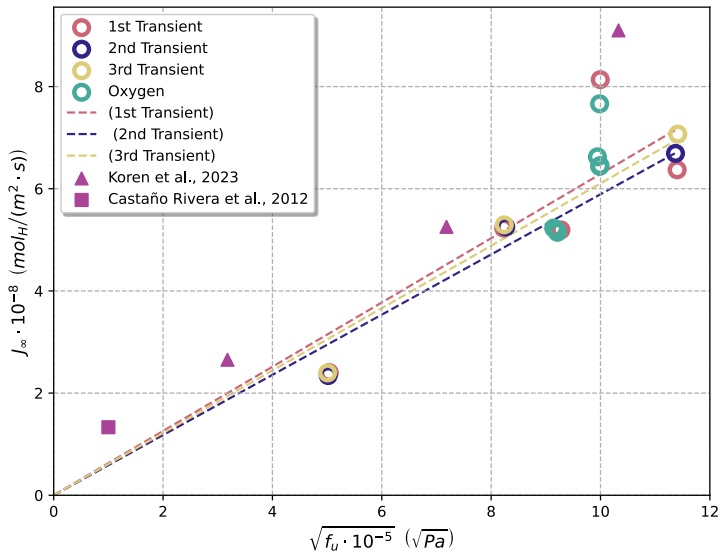

Figure 9 The steady state flux obtained using the balanced model against the square root of fugacity. The linear regression gives the average permeability divided by the sample thickness as the slope of the fitted line. The data in green depict the tests using oxygen.

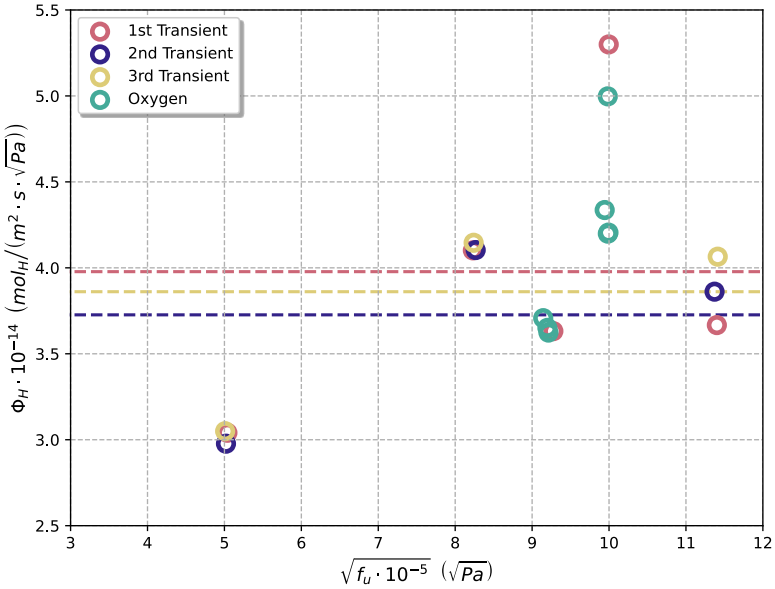

Figure 10 Permeability of each transient is plotted as a function of square root of fugacity. The dashed lines are the average values of permeability evaluated from the slope of the flux times the sample thickness. The permeability evaluated for 25 bar upstream pressure deviates slightly from the average value. Green depicts the tests using oxygen.

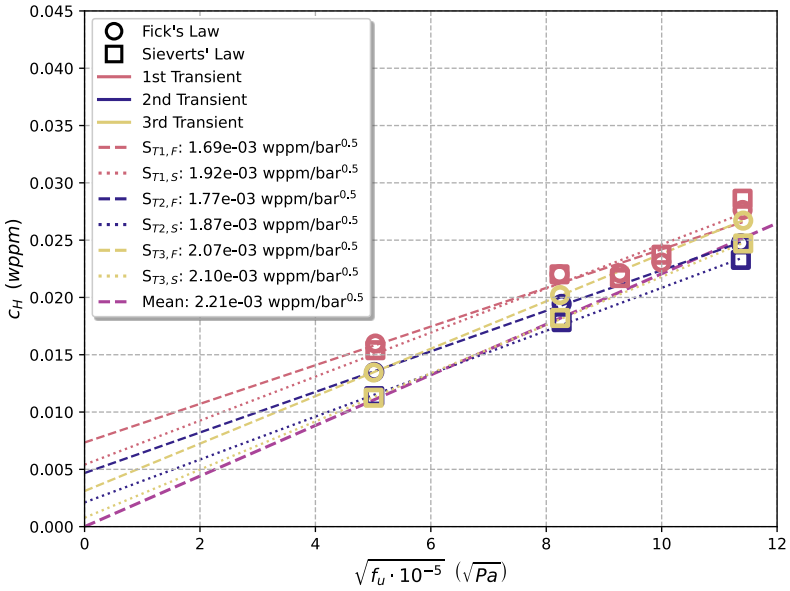

Figure 11 Hydrogen concentration as a function of the square root of fugacity. The dashed lines represent the average solubility constants as evaluated from their respective transients over all pressures using linear regression.

Table 5 Average diffusion parameters evaluated from the linear regression of the third transient.

D (m^2/s)	S ($mol/m^3/Pa^{0.5}$)	($wppm/bar^{0.5}$)	Φ ($mol/m/s/Pa^{0.5}$)	($mol/m/s/bar^{0.5}$)
6.25×10^{-10}	5.45×10^{-5}	2.21×10^{-3}	3.41×10^{-14}	1.08×10^{-11}

4.2 Added Oxygen

In the first set of hydrogen-oxygen experiments, oxygen was introduced to measure its effect on the hydrogen permeation. The oxygen–hydrogen mixture was prepared as described in Section 3.1. When the experiment commenced, oxygen was expanded into the permeation cell first. This was to ensure that oxygen was properly exposed to the specimen. The expected pressure increase due to oxygen expansion was recorded. Subsequently, hydrogen at 81 bar from the hydrogen gas cylinder was expanded into the permeation cell approximately 5 seconds later. The measured hydrogen pressure and the hydrogen flux using hydrogen–oxygen mixture containing 100 ppm, 300 ppm, and 1000 ppm oxygen are presented in Figure 12. The attained steady state hydrogen flux is shown in Figure 9 and the oxygen-influenced permeability is included in Figure 10. A single rise transient at an upstream pressure of 81 bar was conducted using pure hydrogen. This served as an additional baseline result. All oxygen–hydrogen experiments were also conducted using 81 bar total pressure.

Unexpectedly, there was no significant influence of oxygen. The steady state flux as a function of fugacity was comparable to that with the experiments using pure hydrogen. Hence, there was no change in hydrogen permeability due to oxygen. The slight deviation of the steady state flux between the different levels of oxygen was in the range of experimental error. There was no heating between the experiments using different contents of oxygen. This was to keep irreversible traps occupied and because no influence of oxygen was detected.

In the second set of hydrogen-oxygen experiments, the charging sequence was similar to the first set, where oxygen was always charged prior to hydrogen. Hydrogen was sourced from the metal hydride. The measured hydrogen pressure and the hydrogen flux using hydrogen–oxygen mixture at 94 bar containing 100 ppm, 5000 ppm, 12000 ppm oxygen, and exposure to air are presented in Figure 13. Oxygen had a small but measurable effect on the pressure increase, producing lower steady state values of hydrogen flux that decreased with increasing oxygen content. However, there was little to no effect on the onset of hydrogen detection, meaning oxygen functioned as a bottleneck but did not block hydrogen uptake. Figure 14 shows the extended transient for the experiment using 12000 ppm of oxygen. The measured hydrogen flux against the log-time appears to increase linearly, from the apparent steady state value from approximately 2000 s. This might indicate a slowly decaying oxygen reduction at the specimen surface, resulting in an increased steady state flux. The final value of hydrogen flux was close to the steady state hydrogen flux measured in the pure hydrogen baseline experiment at 94 bar. The final experiment was conducted using pure hydrogen. Figure 13 and Figure 14 indicated that the hydrogen flux recovered to the level of the test containing 100 ppm oxygen. This indicates less oxygen was preadsorbed after the test with 12000 ppm oxygen than at the start of the test with 12000 ppm oxygen.

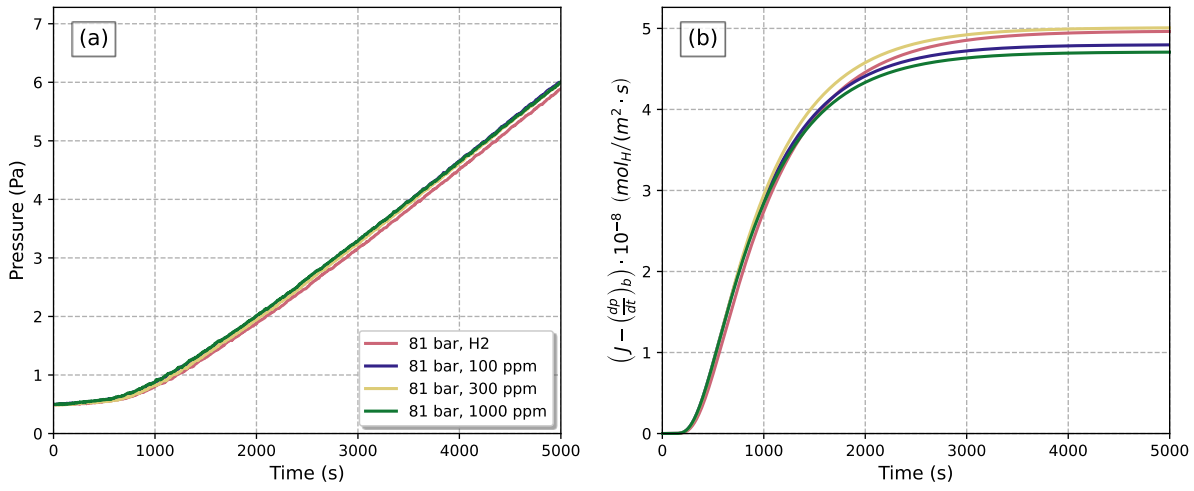

Figure 12 Pressure and flux over time for the first set of experiments with hydrogen-oxygen gas mixtures at 81 bar. There was no influence of the oxygen compared to the baseline run with pure hydrogen. Hydrogen sourced from the hydrogen gas cylinder

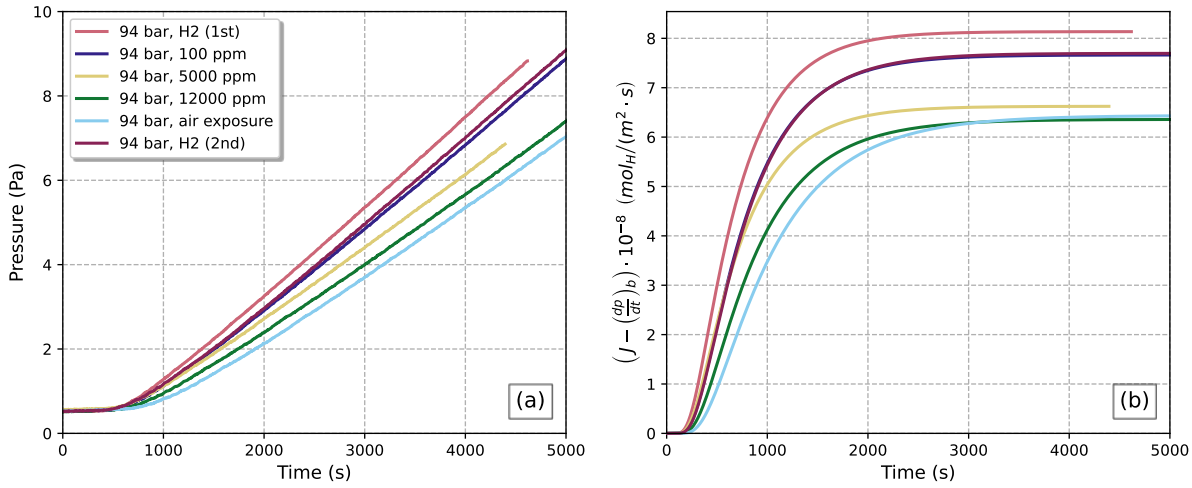

Figure 13 Pressure and flux over time for the second set of experiments with hydrogen-oxygen gas mixtures at 94 bar. Hydrogen sourced from the metal hydride.

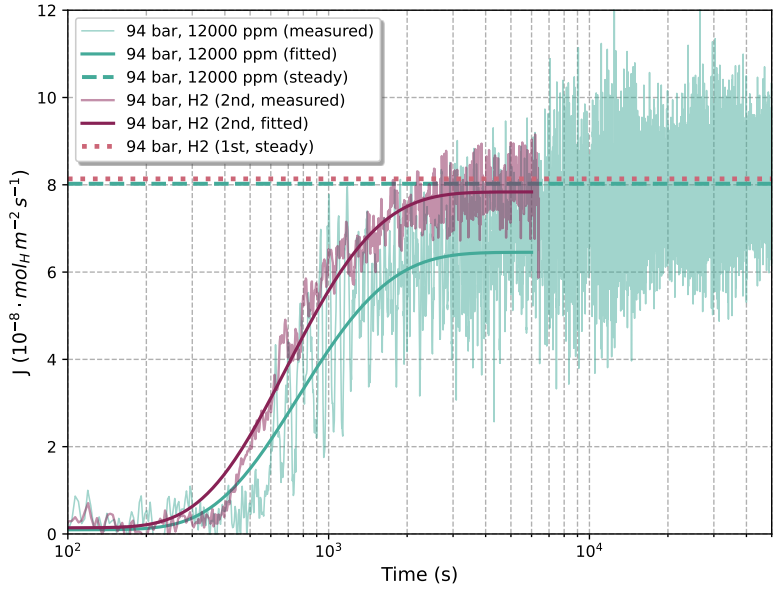

Figure 14 The measured hydrogen flux of the hydrogen-oxygen experiment at 94 bar containing 12000 ppm of oxygen (green, pale underlay). The fitted flux (green, solid line) was evaluated to 5000 s. Thereafter the steady state hydrogen flux slowly increased until reaching the steady state flux of the pure hydrogen baseline experiment at 94 bar. This likely indicated a slow reduction of preadsorbed oxygen to the surface, thereby removing oxygen which led to the recovery of the steady state flux to the value dictated by the membrane permeability and the hydrogen partial pressure. The subsequent experiment using pure hydrogen (purple) showed almost no residual influence of oxygen.

5 DISCUSSION

5.1 Balanced versus Ideal Model

Both models of data fitting were in general agreement. The diffusion parameters obtained by the ideal model are listed in Table 6. Nevertheless, the balanced model provided a better description of the actual experimental conditions used in these experiments. Moreover, whilst the parameters evaluated by each model were similar, the errors associated with the balanced model were significantly smaller. Consequently, the values from the balanced model were to be preferred because the model described the experimental conditions better and the errors were smaller.

It should be mentioned that technically, in the described experimental setup there was no real steady state flux as predicted by Fick's first law. Due to the rise in downstream pressure, Eq. 17 shows that the flux was a function of time (see Figure 5). Nevertheless, as shown using the ideal model, the characteristic of the experimental setup allowed the boundary conditions to be treated as time-invariant. This was due to the low permeability of the steel membrane and the large enough downstream volume. The square root of the downstream pressure, influencing the quasi-steady state flux, was two to three orders of magnitude smaller than the square root of the upstream pressure. Thus, over the course of a typical experiment (5000 – 6000 s), this influence was negligible.

The ideal model fitted the diffusivity to a normalised flux. Therefore, the initial and steady state flux needed to be manually chosen from the measurements. This can introduce a source of error given the noisiness of the flux. Results can deviate significantly for small variations of the initial flux. The balanced model fitted the diffusivity, the solubility constant and the initial flux to the recorded pressure data. The steady state flux was obtained as the maximum flux, predicted by the model. As this could be seen as unambiguous, it was found that these fluxes sometimes deviated from the average values manually chosen for the ideal model. Because the balanced model obtained a best fit over the whole dataset, it may offset the initial and steady flux to match the exponential portion of the transient. However, it is possible to obtain the initial and steady state flux of the balanced model by restricting the solubility constant to be a function of the manually chosen steady state flux using Eq. 17 and 18. The background flux may also be restricted to equate to the initial flux. This way, both models align for downstream pressures significantly smaller than the upstream pressure when the assumption of ideal boundary condition holds.

Table 6 Summary of the diffusion parameter evaluated from rise transients using the ideal model. The normalised root mean square error is based on both the recorded pressure and flux.

Pressure (bar)	Trans.	D_{app} (10^{-10} m^2/s)	S (10^{-5} $mol/m^3/Pa^{0.5}$)	Φ (10^{-14} $mol/m/s/Pa^{0.5}$)	J_∞ (10^{-8} $mol/m^2/s$)	J_b (10^{-9} $mol/m^2/s$)	NRMS (%) p	J
121	1	5.55	6.28	3.48	6.51	2.40	0.77	11.0
	2	6.71	5.15	3.46	6.90	6.94	1.36	13.2
	3	6.87	5.48	3.77	7.30	5.09	1.37	10.8
65	1	5.64	6.81	3.84	5.33	3.39	0.57	10.6
	2	7.05	5.46	3.85	5.34	3.04	0.50	12.1
	3	6.14	5.40	3.31	5.38	1.07	1.12	14.4
25	1	3.58	6.70	2.40	2.32	4.10	1.75	13.2
	2	3.93	5.65	2.22	2.38	6.17	1.21	9.4
	3	4.08	5.29	2.15	2.39	6.85	1.27	13.0

The background flux plays a significant role in the balanced model. Though, it was primarily introduced in Eq. 16 to account for the vacuum leakage, it could be used to fit the initial flux for subsequent transients, that were degassed without heating. Judging from the decay transients, Figure 7, the apparent steady state flux did not reach zero, but a value in the vicinity of the initial flux of the previous rise transient. This could be due to slow detrapping of hydrogen at room temperature. As the release of hydrogen from traps is thermally activated, even at room temperature slow desorption could be possible [47]. The increased background flux for subsequent rise transients, compared to the first transient after heating, was significantly higher. This suggests slow hydrogen release after the lattice diffusible hydrogen rapidly desorbed during the decay transient. However, it cannot be entirely ruled out that part of the background flux was due to other factors such as desorption from the inner walls of the downstream volume, O-ring outgassing or other surface effects.

5.2 Hydrogen Concentration

The hydrogen charging concentration was evaluated using Sieverts' law and Fick's law, Figure 11. The hydrogen concentration calculated using Sieverts' law was generally lower, which can be attributed to the influence of the background flux in the balanced model. The fitted solubility constant, that determines the hydrogen concentration according to Sieverts' law, is based on the adjusted steady state flux. Consequently, if the background flux is

assumed to be primarily hydrogen desorbing from the preceding transient, the concentration should be corrected using

$$c_{\mathrm{diff}} = \frac{J_{\mathrm{b}} L}{D} \qquad 20$$

where c_{diff} is the concentration that should be added to the calculated hydrogen concentration c_{H} given by Sieverts' law using the balanced model, and J_{b} is the fitted background flux that is due to the previous transient.

The evaluated hydrogen concentration in this work was generally lower than previously reported [6–8]. Partially, this may be due to the lower steady state flux, Figure 9. However, Hoschke et al. [6] and Koren et al. [7] measured the diffusivity in X65 in the range of 1×10^{-10} m/s^2 and 3×10^{-10} m/s^2. This is considerably lower than the value from the permeation transients measured herein. Inspection of Eq. 11 and 13 reveals that the calculated equilibrium hydrogen concentration is a function of the steady state flux, which in turn is based on the permeability of the membrane and the upstream pressure. Thus, for a given permeability, the solubility constant is higher the slower the diffusion process (smaller diffusivity). This is reflected in an increase in the calculated hydrogen concentration according to Sieverts' law, when the steady state flux is the same. It can only be speculated why the diffusivities measured here and in previous work differ significantly. However, in both prior works, the specimens were palladium-plated. While, it has been shown [45,48,49] that the influence of a thin palladium layer on steel is negligible in terms of the steady state, as well as the transient flux, there is a possibility that a residual oxide layer had formed between the steel surface and the palladium layer during the sample preparation. This may delay the time to reach the steady state, while still attaining a common steady-state flux as dictated by the permeability and upstream pressure. For this reason, the measured steady-state flux may be a better quantity to relate electrochemical and gaseous permeation experiments to determine their charging conditions.

5.3 Influence of Oxygen

The equilibrium hydrogen concentrations in X65 D measured using the gas phase permeability cell using palladium-plated X65 were comparable to the hydrogen concentration measurements using pipeline steels comparable to X65 [6]. This substantiated the methodology used in this study to measure the hydrogen permeability using X65 D.

Hoschke et al. [6] provided a compilation of measurements of the hydrogen concentration in equilibrium with hydrogen gas. That study indicated clearly that a surface oxide on the pipeline steel could prevent the ingress of hydrogen into the pipeline steel specimen from gaseous hydrogen. Venezuela et al. [32] reported a similar effect; that the native surface oxide on a 3.5NiCrMoV steel could prevent entry of any hydrogen into the steel from the hydrogen gas. In that study, Venezuela et al. [32] found that an activation procedure enabled hydrogen entry into the steel from hydrogen gas. The activation procedure was to heat the steel in gaseous hydrogen at pressure at 200 °C, so that the hydrogen could reduce the surface oxide sufficiently quickly to allow hydrogen ingress within a reasonable holding time at temperature in the hydrogen gas. This activation procedure was used in this research presented in this paper.

Zhou et al. [17] studied the effect of oxygen on the permeation of hydrogen through X52 pipeline steel. At a pressure of 60 bar using pure hydrogen, the steady-state flux was double the steady-state flux measured in this work using 121 bar pure hydrogen. Their specimen was nickel plated on the exit side to facilitate easier hydrogen oxidation. Their specimen was pickled after polishing and nickel-plating. The different material (and material preparation) might lead to a higher permeability and thus faster attainment of the steady state than in the X65 steel investigated in this work. However, the time to reach the steady state was in the vicinity of our results, and considerably shorter than previously reported by Koren et al. [7].

In their work, at a content of 35 ppm oxygen in 60 bar hydrogen, the steady state flux decreased by 55 %. An oxygen content of 350 ppm decreased the steady state flux by 97 %. The breakthrough time increased from 571 s in pure hydrogen to 834 s and 963 s with 35 ppm and 350 ppm oxygen, respectively. Both effects indicated a lower concentration gradient, possibly due to a higher activation energy necessary for dissociative adsorption of hydrogen in the presence of oxygen as proposed by Staykov et al. [21] and slower adsorption kinetics.

In contrast, in this work the effect of oxygen on the hydrogen flux was not as pronounced as measured by Zhou et al. [17]. There was no effect at 81 bar and a slight effect at 94 bar. The differences in both sets of experiments were the repeated sample preparation in the glovebox and the use of hydrogen sourced from the metal-hydride reservoir. While the purity of hydrogen should not have a significant effect for the oxygen inhibition experiments, the repeated sample preparation was likely responsible for the higher flux using pure hydrogen and up to 100 ppm of oxygen.

In addition, Figure 14 indicated that the effect of oxygen decreased with time. This indicated that there might have been a decrease in the oxygen concentration in these experiments.

In summary, the present study produced results significantly different to those in the literature. It is worthwhile comparing the present results with those of Zhou et al. [17] , because that study produced a particularly clear set of results. The present study measured (i) a much smaller apparent equilibrium hydrogen solubility and (ii) a much smaller influence of the oxygen content on the hydrogen permeation flux. For example, Zhou et al. [17] measured a steady- state hydrogen permeation rate for X52 pipeline steel corresponding to a 6 MPa upstream hydrogen pressure double that measured in this work using 121 bar hydrogen, indicating a significantly higher hydrogen solubility in X52 than in X65. Furthermore, an oxygen content of 350 ppm in the hydrogen decreased the hydrogen permeation by 97 % in the work of Zhou et al. [17]. In contrast, in the present work, the hydrogen permeation flux decreased by much smaller amounts: (i) by 6 % for an addition of a much greater oxygen content of 1000 ppm oxygen in 81 bar hydrogen in the first series of experiments using pure hydrogen from the hydrogen cylinder, Figure 12, and (ii) by 22 % for an addition of a further much greater oxygen content of 12000 ppm oxygen in 94 bar hydrogen in the second series of experiments using hydrogen from the metal hydride source, Figure 14. Moreover, Figure 14 records that the hydrogen permeation flux for an addition of 12000 ppm oxygen in 94 bar hydrogen in the second series of experiments steadily increased with time until the hydrogen flux was the same as for the transient at 94 bar hydrogen without the oxygen. This indicated that the influence of oxygen on the hydrogen permeation flux was much smaller than expected from the literature, and moreover, the effect of oxygen was transitory and disappeared with sufficient waiting time.

Zhou et al. [17] also found that 350 ppm oxygen in 6 MPa hydrogen caused the fatigue crack growth in X52 to decrease significantly from that in 6 MPa hydrogen, similar to the many studies of oxygen inhibition of fatigue crack growth in hydrogen [20,24,26–28]. This indicates that the study of Zhou et al. [17] can be considered as a worthy comparison study to the present research.

This present study measured a hydrogen concentration significantly lower than that measured for X65 and similar palladium-coated steel specimens. This indicates that there was some effect of the surface oxide in this present study despite the activation procedure used in the present study to remove the surface oxide.

The present study measured an average value of the hydrogen diffusion coefficient, 6.3×10^{-10} m^2/s substantially greater than the majority of those measured in the literature [6], substantially greater than the hydrogen diffusivity, 1.2×10^{-10} m^2/s measured using palladium-plated X65 D in a gas phase permeation cell [6], and at the upper end of the measurements in Hoschke et al. [6] for X65 D equilibrated with electrochemically generated hydrogen at a hydrogen fugacity estimated to be 850 bar. Experimentally, there is nothing that can be done to the specimen to increase the hydrogen diffusivity, except for heat treatment to reduce hydrogen traps. The fact that the activated X65 D specimen in this study gave a hydrogen diffusion coefficient of 6.3×10^{-10} m^2/s, substantially greater than the hydrogen diffusion coefficient, 1.2×10^{-10} m^2/s, measured using palladium-plated X65 D in the same apparatus, seems to be strong evidence that there is an impediment to hydrogen diffusion through the palladium-plated X65 D specimen. One possibility is an oxide layer at the interface between the palladium layer and the steel surface that impeded hydrogen ingress from the palladium into the steel, and thereby caused a lower effective hydrogen diffusion coefficient to be measured.

There are potentially a number of possible reasons why the results of the present study are so significantly different from literature expectations, and in particular to the results produced by Zhou et al. [17] . (1) There is something in the experimental methodology used in the present study that causes the difference in results. (2) The pipeline steel studied X65 in this work is significantly different to the X52 studied previously [17]. (3) The specimen preparation used in this work causes differences in oxygen adsorption. (4) The influence of oxygen adsorption on pipeline steels has complexities greater than expected. These potential reasons are explored in turn.

Methodology. In the present work hydrogen is admitted to the apparatus either as 99.999 % pure hydrogen from a commercial hydrogen cylinder or generated from a metal hydride. The apparatus was assembled from commercial Swagelok stainless steel fittings. The permeation cell was constructed from type A-286 (UNS S66286) iron-nickel-chromium super alloy and was hydrostatically pressure tested to 250 bar. The cell was sealed using a two-stage O-ring design. Two small O-rings sealed the upstream and downstream volume against the disc specimen and the two flanges. A larger O-ring created a seal between the two flanges. The O-rings were made of Viton, a high-temperature-resistant compound. For membranes with low permeability, outgassing of the O-rings and gas permeation through them could significantly affect the measurements over time, so these were outgasses as described in the experimental section. The experimental details of the flushing and evacuation of the upstream hydrogen chamber, and the pressures measured during the gas handing give confidence that the gas mixtures were as expected, that the gases were high purity and there were no extraneous additions. There is nothing that we have been able to identify that would add additional compounds into the upstream hydrogen chamber or could cause removal of oxygen from the upstream hydrogen gas. It is recognized that there is a thermodynamic tendency for oxygen to react with the hydrogen in the upstream chamber of the permeation cell. However, the rate at room temperature is expected to be small. It might be possible that the clean metal surfaces could provide a catalytic surface for the reaction of oxygen with hydrogen. The reversion of the hydrogen flux in Figure 14 with 12000 ppm oxygen to the flux with pure hydrogen might have been caused by catalytic reduction of the oxygen content, however, this seems unlikely as there was not a significant pressure decrease that would have been required if this amount of oxygen had reacted with hydrogen.

Metal hydride. The metal hydride is charged using the hydrogen of 99.999 % purity from the commercial hydrogen cylinder at a slightly elevated temperature and cooled to room temperature. The metal hydride absorbs only hydrogen. The surface of the metal hydride is exposed to vacuum to remove all gas impurities down to an extremely low level. Thereafter, the metal hydride is heated to release extremely pure hydrogen.

X65 and X52. These are similar pipeline steel, with similar compositions. The stated composition, Table 7, of the X52 indicates the possibility of microalloying, similar to X65. The X52 microstructure was equiaxed ferrite plus some pearlite, compared with a banded ferrite–pearlite microstructure for the X65 elongated in the longitudinal pipe direction induced by the pipe production method.

Surface preparation. The X52 specimen was sequentially ground with 240, 600, 1000, 2000 grit papers to produce a mirror finish, pickled in a glove box before specimen mounting in the permeation cell. The X65 specimen was ground in a glove box with 1200 grit under pure argon before assembly into the permeation cell. The X65 surface was activated by heating in pure hydrogen at 200 °C, whereas no such activation was reported for the X52. In the experiments reported herein, the oxygen was admitted first, which would be expected to maximalize the oxygen inhibition effect, but there was only a small oxygen inhibition effect.

Table 7 Composition of the X52 steel in weight percent. The balance is Fe.

C	Si	Mn	P	S	Cr	Mo	Cu	V
0.10	0.33	1.33	0.01	0.002	0.10	0.10	0.038	0.05

There are differences in experimental procedures, that although they appear to be slight may nevertheless be significant. These will be explored in future research.

6 CONCLUSION

In this work, permeation experiments were conducted on X65 D steel using hydrogen and hydrogen–oxygen mixtures at different pressures and contents of oxygen. The aim was to assess the effect of oxygen on the hydrogen permeation. A gas-phase permeation apparatus was built, and a model using the appropriate boundary conditions was derived. The findings include:

- The derived balanced model of hydrogen permeation could reliably predict the measured permeation transients. The experimental parameters would allow the use of the ideal boundary conditions.

- The measured hydrogen concentration was considerably lower than previously reported. This was likely due to the higher diffusivity. However, the measured steady state fluxes were only slightly lower than in previous works.
- There was no effect of oxygen in the first set of experiments at 81 bar.
- There was a slight effect of oxygen in the second set of experiments at 94 bar. The steady state flux was initially lower compared to pure hydrogen at the same pressure. However, the steady state flux slowly increased back to the level of pure hydrogen.

The low hydrogen concentration evaluated in this work could have been due to a lower steady state flux due to an oxide layer. However, the diffusion process was significantly faster. Furthermore, an already existing oxide layer might influence the detectability of the effect of oxygen on the hydrogen permeation. Future experiments should use a standardised method of specimen preparation that will effectively remove any residual oxide layer.

Acknowledgements

This work is funded by the Future Fuels Cooperative Research Centre research projects RP3.1-13 “Feasibility of the use of gas phase inhibition of hydrogen embrittlement in gas transmission pipelines carrying hydrogen”, supported through the Australian Government’s Cooperative Research Centres Program. The cash and in-kind support from the industry participants is gratefully acknowledged.

CRediT Author Statement

Maximilian Röthig: Conceptualization, Methodology, Formal analysis, Investigation, Data curation, Visualisation, Writing – Original Draft, Writing – Review and Editing,

Joshua Hoschke: Methodology, Writing – Review and Editing,

Clotario V. Tapia-Bastidas: Methodology, Writing – Review and Editing,

Md Fahdul Wahab Chowdhury: Writing – Review and Editing,

Jeffrey Venezuela: Methodology, Writing – Review and Editing, Supervision,

Evan Gray: Conceptualization, Methodology, Writing – Review and Editing, Supervision,

Tom Depover: Writing – Review and Editing,

Kim Verbeken: Writing – Review and Editing,

Milos B. Djukic: Writing – Review and Editing,

Andrej Atrens: Conceptualization, Methodology, Writing – Review and Editing, Supervision, Funding acquisition.

References

[1] J. Hoschke, M.F.W. Chowdhury, J. Venezuela, A. Atrens, A review of hydrogen embrittlement in gas transmission pipeline steels, Corros. Rev. 41 (2023). https://doi.org/10.1515/corrrev-2022-0052.

[2] M.F.W. Chowdhury, C.V. Tapia-Bastidas, J. Hoschke, J. Venezuela, A. Atrens, A review of influence of hydrogen on fracture toughness and mechanical properties of gas transmission pipeline steels, Int. J. Hydrog. Energy 102 (2025) 181–221. https://doi.org/10.1016/j.ijhydene.2025.01.018.

[3] N. Nanninga, A. Slifka, Y. Levy, C. White, A Review of Fatigue Crack Growth for Pipeline Steels Exposed to Hydrogen, J. Res. Natl. Inst. Stand. Technol. 115 (2010) 437–452. https://doi.org/10.6028/jres.115.030.

[4] M.R. Louthan, Hydrogen Embrittlement of Metals: A Primer for the Failure Analyst, J. Fail. Anal. Prev. 8 (2008) 289–307. https://doi.org/10.1007/s11668-008-9133-x.

[5] P. Lam, A. Andrew Duncan, R. Robert Sindelar, T. Thad Adams, Literature Survey of Gaseous Hydrogen Effects on the Mechanical Properties of Carbon and Low Alloy Steels, ASME J. Press. Vessel Technol. (2009). https://doi.org/10.1115/1.3141435.

[6] J. Hoschke, M. Roethig, C.V. Tapia-Bastidas, M.F.W. Chowdhury, J. Venezuela, Y. Shu, E. Gray, A. Atrens, Determination of the hydrogen fugacity during cathodic hydrogen charging of X65 D pipeline steel, Corros. Sci. 243 (2025) 112580. https://doi.org/10.1016/j.corsci.2024.112580.

[7] E. Koren, C. M. H. Hagen, D. Wang, X. Lu, R. Johnsen, J. Yamabe, Experimental comparison of gaseous and electrochemical hydrogen charging in X65 pipeline steel using the permeation technique, Corros. Sci. 215 (2023) 111025. https://doi.org/10.1016/j.corsci.2023.111025.

[8] E. Koren, J. Yamabe, X. Lu, C.M.H. Hagen, D. Wang, R. Johnsen, Hydrogen diffusivity in X65 pipeline steel: Desorption and permeation studies, Int. J. Hydrog. Energy 61 (2024) 1157–1169. https://doi.org/10.1016/j.ijhydene.2024.03.027.

[9] M.F.W. Chowdhury, C.V. Tapia-Bastidas, J. Hoschke, J. Venezuela, T. Liu, M.B. Djukic, T. Depover, K. Verbeken, L. Mcinnes, M. Roethig, A. Karimi, A. Atrens, Preliminary Evaluation of the Influence of Hydrogen on the Fracture Toughness of an X65 Gas-Transmission Pipeline Steel, Adv. Eng. Mater. 26 (2024) 2400352. https://doi.org/10.1002/adem.202400352.

[10] M.F.W. Chowdhury, C.V. Tapia-Bastidas, J. Hoschke, J. Venezuela, M. Roethig, A. Atrens, Influence of hydrogen fugacity on the fracture toughness and fracture mechanism of a X65 natural gas transmission pipeline steel, Int. J. Hydrog. Energy 89 (2024) 1415–1429. https://doi.org/10.1016/j.ijhydene.2024.09.035.

[11] J. Hoschke, M.F.W. Chowdhury, J. Venezuela, C.V. Tapia-Bastidas, M. Roethig, L. Lan, A. Atrens, Influence of hydrogen on the tensile properties of X65 D pipeline steel, Int. J. Hydrog. Energy 101 (2025) 538–555. https://doi.org/10.1016/j.ijhydene.2024.12.410.

[12] ASME B31.12-2019, Hydrogen Piping and Pipelines: ASME Code for Pressure Piping, B31, (2019).

[13] J.H. Holbrook, H.J. Cialone, E.W. Collings, E.J. Drauglis, P.M. Scott, M.E. Mayfield, Control of hydrogen embrittlement of metals by chemical inhibitors and coatings, in: Gaseous Hydrog. Embrittlement Mater. Energy Technol., Elsevier, 2012: pp. 129–153. https://doi.org/10.1533/9780857095374.1.129.

[14] Y. Lei, E. Hosseini, L. Liu, C.A. Scholes, S.E. Kentish, Internal polymeric coating materials for preventing pipeline hydrogen embrittlement and a theoretical model of hydrogen diffusion through coated steel, Int. J. Hydrog. Energy 47 (2022) 31409–31419. https://doi.org/10.1016/j.ijhydene.2022.07.034.

[15] A. Atrens, E. Gray, J. Venezuela, J. Hoschke, M. Roethig, Feasibility of the Use of Gas Phase Inhibition of Hydrogen Embrittlement in Gas Transmission Pipelines Carrying Hydrogen: A Review, JOM (2022). https://doi.org/10.1007/s11837-022-05559-8.

[16] M. Röthig, J. Hoschke, C. Tapia, J. Venezuela, A. Atrens, A review of gas phase inhibition of gaseous hydrogen embrittlement in pipeline steels, Int. J. Hydrog. Energy 60 (2024) 1239–1265. https://doi.org/10.1016/j.ijhydene.2024.02.245.

[17] C. Zhou, H. Zhou, L. Zhang, The Impact of Impurity Gases on the Hydrogen Embrittlement Behavior of Pipeline Steel in High-Pressure H2 Environments, Materials 17 (2024) 2157. https://doi.org/10.3390/ma17092157.

[18] C. Wang, X. Xu, Y. Hua, R. Zhang, C. Liu, X. Luo, S. Gu, Y. Li, Y.F. Cheng, Inhibiting effect of carbon monoxide on gaseous hydrogen embrittlement of pipelines transporting hydrogen, Corros. Sci. 227 (2024) 111789. https://doi.org/10.1016/j.corsci.2023.111789.

[19] E. Protopopoff, P. Marcus, Surface Effects on Hydrogen Entry into Metals, in: Corros. Mech. Theory Pract., CRC Press, 2011: pp. 105–148.

[20] J. Holbrook, E. Collings, H. Cialone, E. Drauglis, Hydrogen degradation of pipeline steels: Final report, Battelle Columbus Laboratories, 1986. https://doi.org/10.2172/7122938.

[21] A. Staykov, J. Yamabe, B.P. Somerday, Effect of hydrogen gas impurities on the hydrogen dissociation on iron surface, Int. J. Quantum Chem. 114 (2014) 626–635. https://doi.org/10.1002/qua.24633.

[22] W. Hofmann, W. Rauls, Ductility of Steel Under the Influence of External High Pressure Hydrogen, Weld. J. Res. Suppl. 44 (1965) 225s–230s.

[23] H. Barthélémy, G.M. Pressouyre, Hydrogen gas embrittlement of steels: synthesis of a subtask of the CEC hydrogen energy programme (1975-83) : final report, Commission of the European Communities, Directorate-General Science, Research and Development, Luxembourg, 1985.

[24] H.J. Cialone, J.H. Holbrook, Sensitivity of Steels to Degradation in Gaseous Hydrogen, in: L. Raymond (Ed.), Hydrog. Embrittlement Prev. Control, ASTM International, 100 Barr Harbor Drive, PO Box C700, West Conshohocken, PA 19428-2959, 1988: pp. 134–152. https://doi.org/10.1520/STP45297S.

[25] K. Kussmaul, P. Deimel, E. Sattler, Tensile Properties of the Steel X 70 TM in High Pressure Hydrogen Gas with Admixtures of Oxygen at Different Strain Rates, in: Hydrog. Energy Prog. X Proc. 10th World Energy Conf., Pergamon, 1994: pp. 285–294.

[26] P. Deimel, H. Fischer, E. Sattler, M. Hoffmann, Fracture Mechanics in High Pressure Hydrogen for the Thermomechanically Treated Steel X70, in: T.O. Saetre (Ed.), Hydrog. Power Theor. Eng. Solut., Springer Netherlands, Dordrecht, 1998: pp. 331–336. https://doi.org/10.1007/978-94-015-9054-9_43.

[27] B.P. Somerday, P. Sofronis, K.A. Nibur, C. San Marchi, R. Kirchheim, Elucidating the variables affecting accelerated fatigue crack growth of steels in hydrogen gas with low oxygen concentrations, Acta Mater. 61 (2013) 6153–6170. https://doi.org/10.1016/j.actamat.2013.07.001.

[28] J. Ronevich, C. San Marchi, R. Kolasinski, K. Thurmer, N. Bartelt, F. El Gabaly, B. Somerday, Oxygen Impurity Effects on Hydrogen Assisted Fatigue and Fracture of X100 Pipeline Steel, in: Proc. ASME 2018 Press. Vessels Pip. Conf., American Society of Mechanical Engineers Digital Collection, 2018: p. V06BT06A027. https://doi.org/10.1115/PVP2018-84163.

[29] R. Komoda, M. Kubota, A. Staykov, P. Ginet, F. Barbier, J. Furtado, Inhibitory effect of oxygen on hydrogen-induced fracture of A333 pipe steel, Fatigue Fract. Eng. Mater. Struct. 42 (2019) 1387–1401. https://doi.org/10.1111/ffe.12994.

[30] S.P. Lynch, Hydrogen embrittlement (HE) phenomena and mechanisms, in: Stress Corros. Crack., Elsevier, 2011: pp. 90–130. https://doi.org/10.1533/9780857093769.1.90.

[31] W.G. Perkins, Permeation and Outgassing of Vacuum Materials, J. Vac. Sci. Technol. 10 (1973) 543–556. https://doi.org/10.1116/1.1318061.

[32] J. Venezuela, C. Tapia-Bastidas, Q. Zhou, T. Depover, K. Verbeken, E. Gray, Q. Liu, Q. Liu, M. Zhang, A. Atrens, Determination of the equivalent hydrogen fugacity during electrochemical charging of 3.5NiCrMoV steel, Corros. Sci. 132 (2018) 90–106. https://doi.org/10.1016/j.corsci.2017.12.018.

[33] J.G. Speight, Handbook of Natural Gas Analysis, John Wiley & Sons, 2018. https://app.knovel.com/hotlink/toc/id:kpHNGA0001/handbook-natural-gas/handbook-natural-gas.

[34] A. Fick, Ueber Diffusion, Ann. Phys. 170 (1855) 59–86. https://doi.org/10.1002/andp.18551700105.

[35] M. a. V. Devanathan, Z. Stachurski, F.C. Tompkins, The adsorption and diffusion of electrolytic hydrogen in palladium, Proc. R. Soc. Lond. Ser. Math. Phys. Sci. 270 (1962) 90–102. https://doi.org/10.1098/rspa.1962.0205.

[36] J. Crank, The mathematics of diffusion, 2d ed, Clarendon Press, Oxford, [Eng], 1975.

[37] American Society of Mechanical Engineers, ASTM G148 - 97(2018), Standard Practice for Evaluation of Hydrogen Uptake, Permeation, and Transport in Metals by an Electrochemical Technique, (2018).

[38] H.A. Daynes, S.W.J. Smith, The process of diffusion through a rubber membrane, Proc. R. Soc. Lond. Ser. Contain. Pap. Math. Phys. Character 97 (1920) 286–307. https://doi.org/10.1098/rspa.1920.0034.

[39] R.M. Barrer, E.K. Rideal, Permeation, diffusion and solution of gases in organic polymers, Trans. Faraday Soc. 35 (1939) 628–643. https://doi.org/10.1039/TF9393500628.

[40] B.S. Chaudhari, T.P. Radhakrishnan, On hydrogen diffusivity in metals from electropermeation transients, Surf. Technol. 22 (1984) 353–366. https://doi.org/10.1016/0376-4583(84)90099-2.

[41] H.S. Carslaw, Introduction to the Theory of Fourier's Series and Integrals, Third, Macmillan and Co., Ltd., London, 1923.

[42] A. Sieverts, The Absorption of Gases by Metals, Z. Für Met. 21 (1929) 37–46.

[43] C. San Marchi, B.P. Somerday, S.L. Robinson, Permeability, solubility and diffusivity of hydrogen isotopes in stainless steels at high gas pressures, Int. J. Hydrog. Energy 32 (2007) 100–116. https://doi.org/10.1016/j.ijhydene.2006.05.008.

[44] T. Zakroczymski, Adaptation of the electrochemical permeation technique for studying entry, transport and trapping of hydrogen in metals, Electrochimica Acta 51 (2006) 2261–2266. https://doi.org/10.1016/j.electacta.2005.02.151.

[45] A.J. Kumnick, H.H. Johnson, Steady state hydrogen transport through zone refined irons, Metall. Trans. A 6 (1975) 1087–1091. https://doi.org/10.1007/BF02661363.

[46] K. Kiuchi, R.B. McLellan, The solubility and diffusivity of hydrogen in well-annealed and deformed iron, Acta Metall. 31 (1983) 961–984. https://doi.org/10.1016/0001-6160(83)90192-X.

[47] H.E. Kissinger, Reaction Kinetics in Differential Thermal Analysis, Anal. Chem. 29 (1957) 1702–1706. https://doi.org/10.1021/ac60131a045.

[48] J.A. Barrie, J.D. Levine, A.S. Michaels, P. Wong, Diffusion and solution of gases in composite rubber membranes, Trans. Faraday Soc. 59 (1963) 869–878. https://doi.org/10.1039/TF9635900869.

[49] R. Ash, R.M. Barrer, D.G. Palmer, Diffusion in multiple laminates, Br. J. Appl. Phys. 16 (1965) 873. https://doi.org/10.1088/0508-3443/16/6/314.